

Spatially-explicit modeling improves empirical characterization of dispersal: theory and a case study

Petteri Karisto^{1†}, Frédéric Suffert², and Alexey Mikaberidze^{1‡}

¹ Plant Pathology Group, Institute of Integrative Biology, ETH Zurich, Zurich, Switzerland.

² INRA, Agro Paris Tech, UMR 1290 BIOGER-CPP, Thiverval-Grignon, France.

[†] present address: Department of Evolutionary Biology and Environmental Studies,
University of Zurich, Zurich, Switzerland.

[‡] present address: School of Agriculture, Policy and Development, University of Reading,
Whiteknights, Reading, UK.

Corresponding author: P. Karisto

Email address: petteri.karisto@ieu.uzh.ch

Keywords: Dispersal kernel, Dispersal gradient, Source geometry, *Zymoseptoria tritici*,

Rain-splash dispersal, Bootstrap

Content:

Abstract

Main text

Appendices A, B, C, and D.

6700 words in the main text.

20

Abstract

Dispersal is a key ecological process. An individual dispersal event has a source and a destination, both are well localized in space and can be seen as points. A probability to move from a source point to a destination point can be described by a dispersal kernel. However, when we measure dispersal, the source of dispersing individuals is usually an area, which distorts the shape of the dispersal gradient compared to the dispersal kernel. Here, we show theoretically how different source geometries affect the gradient shape depending on the type of the kernel. We present an approach for estimating dispersal kernels from measurements of dispersal gradients independently of the source geometry. Further, we use the approach to achieve the first field measurement of dispersal kernel of an important fungal pathogen of wheat, *Zymoseptoria tritici*. Rain-splash dispersed asexual spores of the pathogen spread on a scale of one meter. Our results demonstrate how analysis of dispersal data can be improved to achieve more rigorous measures of dispersal. Our findings enable a direct comparison between outcomes of different experiments, which will allow to acquire more knowledge from a large number of previous empirical studies of dispersal.

36 Introduction

Individuals comprising biological populations often need to move from one location to
38 a different location in order to survive and reproduce. Hence, dispersal is an important
component of many life histories. Empirical characterization of dispersal has been a
40 major theme in ecological research for a long time (for example Heald, 1913; Bullock
et al., 2017). However, Bullock et al. (2017) found much fewer datasets describing plant
42 dispersal than plant demography, likely indicating that “dispersal is notoriously difficult
and resource-consuming to measure”.

44 To measure dispersal, one needs a source of dispersing units and a method to record
their displacement. Sources can be natural (e.g. a spawning site) or artificial (a planted
46 patch). To record the displacement, studies on animal movement often use on mark-
recapture experiments (Van Houtan et al., 2007; Carrasco et al., 2010), while plant
48 studies commonly use seed traps or genotyping of seedlings around potential parents
(Nathan et al., 2000; Goto et al., 2006). Spread of a plant pathogen can be recorded based
50 on visual symptoms and genetic data (Solheim and Hietala, 2017). The appropriate
methodology varies depending on the study system.

52 In the presence of a localized source, a dispersal gradient is expected: many individuals
will stay close to the source while fewer individuals will travel further, leading to a
54 decreasing dependency with distance. This pattern can be described mathematically by
fitting a decreasing one-dimensional function to gradient measurements (e.g. review of
56 Fitt et al., 1987; Ferrandino, 1996; Werth et al., 2006; Madden et al., 2007). However,
the geometry of the source affects the shape of such gradients (Zadoks and Schein,
58 1979; Ferrandino, 1996; Cousens and Rawlinson, 2001). “Flattening” of gradients due
to extended sources is noted qualitatively in previous studies (Zadoks and Schein, 1979;
60 Ferrandino, 1996), but how exactly and how much does the source geometry affect the
dispersal gradient?

62 A more rigorous mathematical description of dispersal is achieved with a dispersal
kernel that represents a probability distribution of dispersal to a certain location relative
64 to the source (“dispersal location kernel”, Nathan et al., 2012). It is convenient to have
a point source for an empirical characterization of dispersal kernels, because a dispersal
66 gradient from a point source will have the same shape as the kernel. Zadoks and Schein
(1979) proposed a rule of thumb, stating that a point source should have “a diameter
68 smaller than 1% of the gradient length; but in many experiments, it is up to 5 or
10%”. However, to determine whether the source is small enough so that the dispersal
70 gradient captures the shape of the dispersal kernel, the size of the source should be
compared with the characteristic distance of dispersal (i.e., the distance over which the
72 dispersal kernel changes substantially), rather than the gradient length. This represents a
challenge for the design of dispersal experiments that aim to achieve a point-like source,
74 because whether or not the chosen source size is sufficiently small can be established
with certainty only when the measurements are already conducted. As a result, “point”
76 sources of various sizes are found in literature: an adult tree (Werth et al. (2006); cf.
Cousens and Rawlinson (2001) presenting effect of tree canopy morphology on the shape
78 of the gradient), circles of 80 cm (Skarpaas and Shea, 2007) and 25 cm diameter (Loebach
and Anderson, 2018), 4 m² square (Emsweller et al., 2018), route of a single sampling
80 dive (D’Aloia et al., 2015).

This challenge can be resolved using a modeling approach that incorporates the spread
82 from any source geometry considering each point within the source as an independent
point source (Clark et al., 1999). This would lead to a better, more mechanistic under-
84 standing of the dispersal as recommended by Bullock et al. (2006). While such approach
has been suggested (e.g. by Greene and Calogeropoulos, 2002) it is rarely adopted, as
86 demonstrated by the previous examples of various “point” sources and, for example, Bul-
lock et al. (2017) who excluded line and area sources from their analysis, because those

88 could not be compared to gradients from point sources.

We investigate the effect of source geometry on the shape of dispersal gradients consid-
90 ering three qualitatively different dispersal kernels: exponential, Gaussian, and power-
law. We present possible simplifications, i.e. cases when a non-point source can be con-
92 sidered a point. We provide straightforward mathematical methods to take into account
the source geometry in a more general case, when the simplifications are not possible.
94 Finally, we present results of a case study, where we measured rain-splash driven asexual
dispersal of a major fungal pathogen of wheat, *Zymoseptoria tritici*, characterizing its
96 dispersal kernel for the first time in natural, field conditions.

Theory

98 Dispersal location kernel describes the probability of dispersal from a source point
($p_s = (x_s, y_s)$) to a destination point ($p_d = (x_d, y_d)$) depending on the distance be-
100 tween the points ($r(p_s, p_d) = \sqrt{(x_d - x_s)^2 + (y_d - y_s)^2}$). Note the important difference
between dispersal location kernel and dispersal distance kernel (Appendix A); we con-
102 sider dispersal location kernel hereafter. In an ideal situation, the dispersal kernel could
be measured in an experiment with a similar structure: a single point as a source of
104 dispersing individuals and a single point for measuring dispersed individuals at each
location. In such an experiment, the dispersal gradient, i.e. the spatial distribution of
106 the dispersed individuals will correspond to the dispersal kernel. In reality, the source or
the destination or both are usually areas, i.e. the source has a certain measurable area
108 and the measurements at the destination are performed over a certain area. To describe
such situations mathematically, we have to take sum over the individual points com-
110 prising the source to calculate their combined contribution to the dispersing population.
Similarly, the sum over all points of the destination area gives the total population in

112 the area. Population in a destination area D after dispersal is then calculated as

$$N_1(S, D) = \iint_D \iint_S N_0(p_s) \kappa(r) dA_S dA_D \quad (1)$$

114 where $N_0(p_s)$ is the total dispersing population from p_s (more precisely, the density
function of the dispersing individuals within S), $S = \{p_s\}$ is the source area, $\kappa(r)$ is
116 the dispersal kernel, and area integrals sum up the contributions of source points and
destination points to the total observed population at the destination $D = \{p_d\}$. When
118 the populations before dispersal (N_0) and after dispersal (N_1) are measured, the Eq. (1)
becomes the function of only the kernel parameters, which can be estimated by fitting
120 this function to the data.

Fitting a model with the above structure to empirical data can be challenging. Mul-
122 tiple integrations increase the computational demand making the process slower. Also,
analytical solutions are more difficult to achieve with complex formulae. Therefore, sim-
124 plifications could be useful to improve the analytical understanding and data analysis.

A common simplification is to fit a one-dimensional model to dispersal gradient data to
126 estimate dispersal without accounting for the source geometry: $N_1 = C\kappa$. For example,
a function of the form

$$128 \quad N_1 = Ce^{-x/\alpha} \quad (2)$$

can be used to estimate the dispersal parameter α and the scale parameter C , in the case
130 of an exponential kernel. The parameter C here does not have a clear biological meaning.
If both the source and the destination are points, the above approach provides a correct
132 estimate for the dispersal parameter α , because the function in Eq. (2) is the same as the
exponential dispersal kernel [Eq. (3) in Box 1] up to a constant factor. The estimate of
134 the parameter C then contains the normalization factor of the kernel and other biological
parameters, such as the population size at the source and the dispersal probability, which

Exponential kernel is defined as

$$\kappa_e(r, \alpha) = C_k e^{-r/\alpha} \quad (3)$$

where $k \in \{1, 2\}$ is the number of dimensions, $r = r(p_s, p_d) > 0$ is the Euclidean distance from the source point $p_s = (x_s, y_s)$ to the destination point $p_d = (x_d, y_d)$ (in one dimension $y_s = y_d = 0$), and C_k is normalization factor: $C_1 = 1/(2\alpha)$ and $C_2 = 1/(2\pi\alpha^2)$.

Gaussian kernel is defined as

$$\kappa_g(r, \alpha) = C_k e^{-r^2/2\alpha^2}, \quad (4)$$

where $C_1 = 1/\sqrt{2\pi\alpha^2}$ and $C_2 = 1/(\pi\alpha^2)$.

Power-law kernel is defined here as

$$\kappa_p(r, \alpha, \lambda) = C_k (\lambda + r)^{-\alpha}, \quad (5)$$

where $C_1 = (\alpha - 1)\lambda^{\alpha-1}$, $C_2 = (\alpha - 2)(\alpha - 1)\lambda^{\alpha-2}/(2\pi)$. λ is a scale parameter defining the finite starting point of the distribution in relation to $r^{-\alpha}$ distribution, which is not defined at $r = 0$.

Box 1

136 cannot be disentangled without additional information. This approach generally works
 for any kernel function (e.g., Gaussian or power-law kernels), when both the source and
 138 the destination are points.

However, when the geometry of the source and/or destination is more complex, the
 140 above approach may lead to wrong estimates. The parameter α estimated with this
 approach, may depend on the particular experimental design and have no relation to
 142 the actual kernel shape. However, the shape of the dispersal gradient does match to
 the shape of the dispersal kernel even when the source and the destination are areas in
 144 certain special cases. We discuss these special cases in relation to exponential, Gaussian,
 and power-law kernels (defined in Box 1).

146 If the source is extended in the direction of the measured gradient, and the underlying
 kernel is exponential, the Eq. (2) will still give a correct estimate of α . This holds,
 148 because exponential kernels are memoryless (Box 2). This property allows to sum up
 all point sources within the source area along the x -axis to an equivalent virtual point

Memoryless kernel. Exponential kernels have a special feature: they are memoryless. To be memoryless means that setting any point along the gradient as a starting point, the tail of the distribution will have the same shape as entire distribution. This property explains why exponential kernel can be described unambiguously with the half-distance $\alpha \ln(2)$. From any point on an exponential gradient, moving $\alpha \ln(2)$ further along the gradient will decrease the density by half.

Separable kernel. Separable functions are those that can be expressed as a product of functions which depend on only one independent variable each, e.g. $f(x, y) = f_x(x)f_y(y)$. The shape of the dispersal gradient in the x -direction does not depend on the y -coordinate if the kernel is separable.

Most dispersal kernels found in the literature are neither memoryless nor separable (Nathan et al., 2012).

Box 2

150 source at $x = 0$ and in this way simplify the fitting process (see Fig. 1B). Thus, the
extension of the source in the direction of the gradient will only add more power to
152 the source but not change the shape of the gradient outside of the source, leading to a
correct estimate of α . This is not true for Gaussian and power-law kernels (Fig. 1 C, D).

154 If the extension of the source is in the other direction, perpendicular to the source, the
simplified approach works with Gaussian kernel (Fig. 1C). Gaussian kernel is separable,
156 which means that the shape of the kernel along x -dimension does not change when y_s
varies (Box 2). Hence, when measuring the dispersal along the x -axis, the extension of
158 source along the y -axis only adds to the power of the source but does not modify shape of
the gradient. Thus changing the source from a point to a thin line source perpendicular
160 to the gradient leads to a different estimate of C but the same estimate of α . This holds
for any separable kernel, but not for non-separable exponential or power-law kernels
162 (Fig. 1B, D).

The situation is analogous when we consider extended destinations. Extended des-
164 tination here implies that multiple measurements are conducted across the destination
area in a uniformly random manner, and subsequently an average is taken over these

166 measurements. When the kernel is exponential, both the source and the destination
can be elongated in the direction of the dispersal gradient. An exponential function in
168 Eq. (2) fitted to dispersal gradient data acquired in this way will have same dispersal
parameter α as the dispersal kernel. In the case of separable kernels, both the source
170 and the destination can be elongated perpendicular to the gradient and the gradient
will have the same shape as the original kernel. If the geometry of the source or the
172 destination is more complex, for example rectangles, the presented simplifications fail
with each of the three kernels.

174 Case study

Materials and methods of the experiment

176 Experimental design and disease measurements

We performed a field experiment to measure dispersal kernels of *Zymoseptoria tritici* in
178 natural, field conditions within a wheat canopy. By analyzing the experimental data
we demonstrate both benefits and drawbacks of simplifications related to the theory
presented above. Winter wheat cultivar Runal was grown in $1.125\text{ m} \times 4\text{ m}$ plots in
180 Eschikon, Switzerland (coordinates: 47.449N, 8.682E). Inoculation was performed in
inoculation areas in the middle of each plot (Fig. 2 A) on 17–18 May 2017 with 300 ml
of spore suspension containing 10^6 spores/ml of *Z. tritici* strain 1A5 (treatment A), strain
184 3D7 (D) or both strains (B, 5×10^5 sp/ml each) (Zhan et al., 2002). The pathogen strains
were chosen because of their capacity to infect cultivar Runal and due to their contrasting
186 production of pycnidia (asexual fruiting bodies) (Stewart et al., 2018). Control plots
(C) were not inoculated. Five replicates of each treatment were assigned in a fully
188 randomized design to 20 plots (Fig. B1). Further details of the experimental materials
and methods are given in the Appendix B.

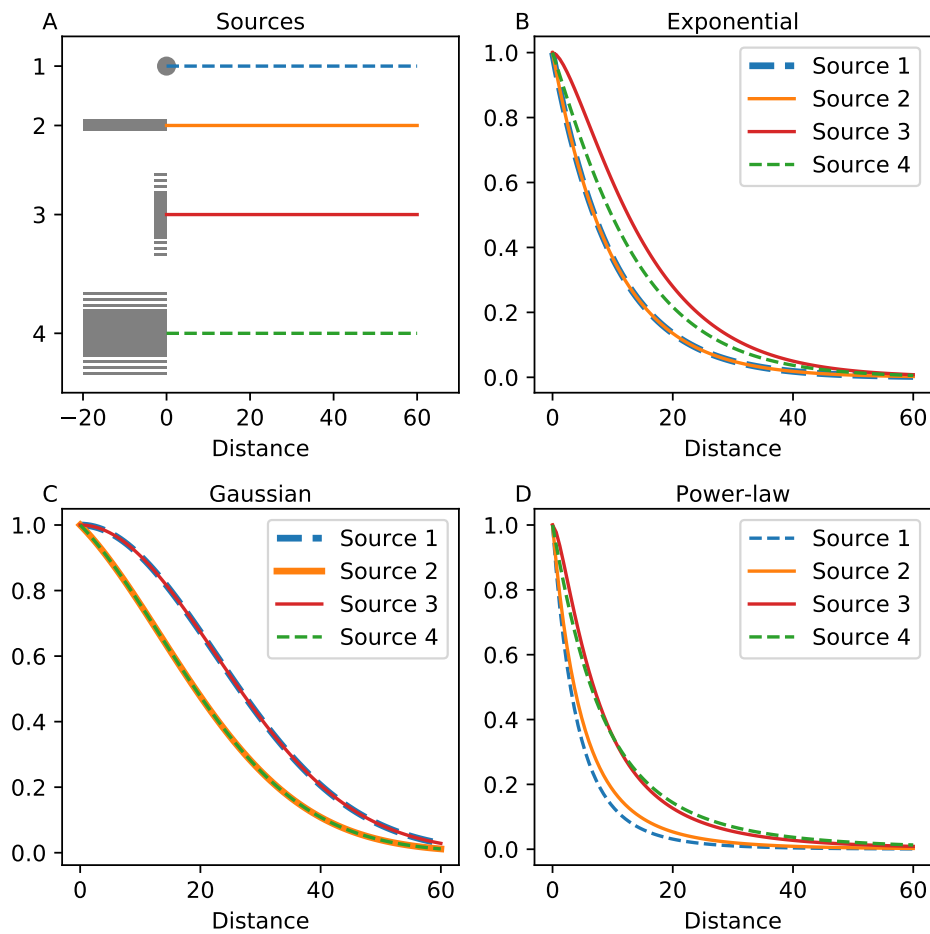


Figure 1: How source geometry affects the shape of dispersal gradients with different kernels (Box 1). (A) Four different sources: 1) point source; 2) Line source $x \in [-20, 0]$; 3) Line source, $y \in [-100, 100]$; 4) Rectangular area source, $(x, y) \in [-20, 0] \times [-100, 100]$. (B, C, D) Simulated gradients along the coloured lines in (A). Kernel parameters are chosen such that the mean dispersal distance is 20 units in all cases. Gradients are normalized to begin at 1. (B) With the exponential kernel ($\alpha = 10$), sources 1 and 2 result in identical gradients. (C) With the Gaussian kernel ($\alpha = 22.5$) the gradients are identical between sources 1 and 3 and between sources 2 and 4. (D) With the power-law kernel ($\alpha = 5, \lambda = 20$) all gradients are different.

190 Disease levels were measured within 10 cm-wide measurement lines across each plot
(Fig. 2A), representing the destination area. Within each measurement line, multiple
192 measurements were conducted in a uniformly random manner. In each measurement, *Z.
tritici* incidence was assessed at the leaf scale by visual counting. After that, diseased
194 leaves were collected and analyzed using the automated image analysis (Karisto et al.,
2018, and Fig. 2 B-D) to obtain pycnidia counts as a measure of conditional severity.
196 Success of inoculation was confirmed within the inoculated areas (source areas) on 14
June and primary disease gradients were measured in all measurement lines three weeks
198 later, on 4 July.

Statistical analysis

200 **Fitting disease gradients.** The disease intensity (numbers of pycnidia per leaf) at t_1
in a given measurement line is a result of dispersal of spores and successful infections
202 from the source area to the area of the measurement line (i.e. the destination area).
Assuming spatially uniform success of infections in all plots, the observed disease gradient
204 is the result of the dispersal gradient of spores and it provides the effective dispersal
gradient of the pathogen population. Following the equation (1) with the exponential
206 kernel (that fits well when dispersal is driven by water splashes, according to Fitt et al.,
1987; Saint-Jean et al., 2004), the dispersal process of the pathogen can be described
208 mathematically using two area integrals: one over the source area and the other over
the destination area. The disease intensity at the time t_1 in a measurement line at a
210 distance x^* (destination $D = \{(x_d, y_d)\} = [x^* - 5, x^* + 5] \times [b, w - b]$) from the inoculation
area (source $S = \{(x_s, y_s)\} = [0, 40] \times [0, w]$) is given by

$$212 \quad I_{t_1}(x^*) = \frac{I_0\beta}{10(w-2b)} \iint_D \iint_S \frac{e^{-\sqrt{(x_d-x_s)^2+(y_d-y_s)^2}/\alpha}}{2\pi\alpha^2} dA_S dA_D \quad (6)$$

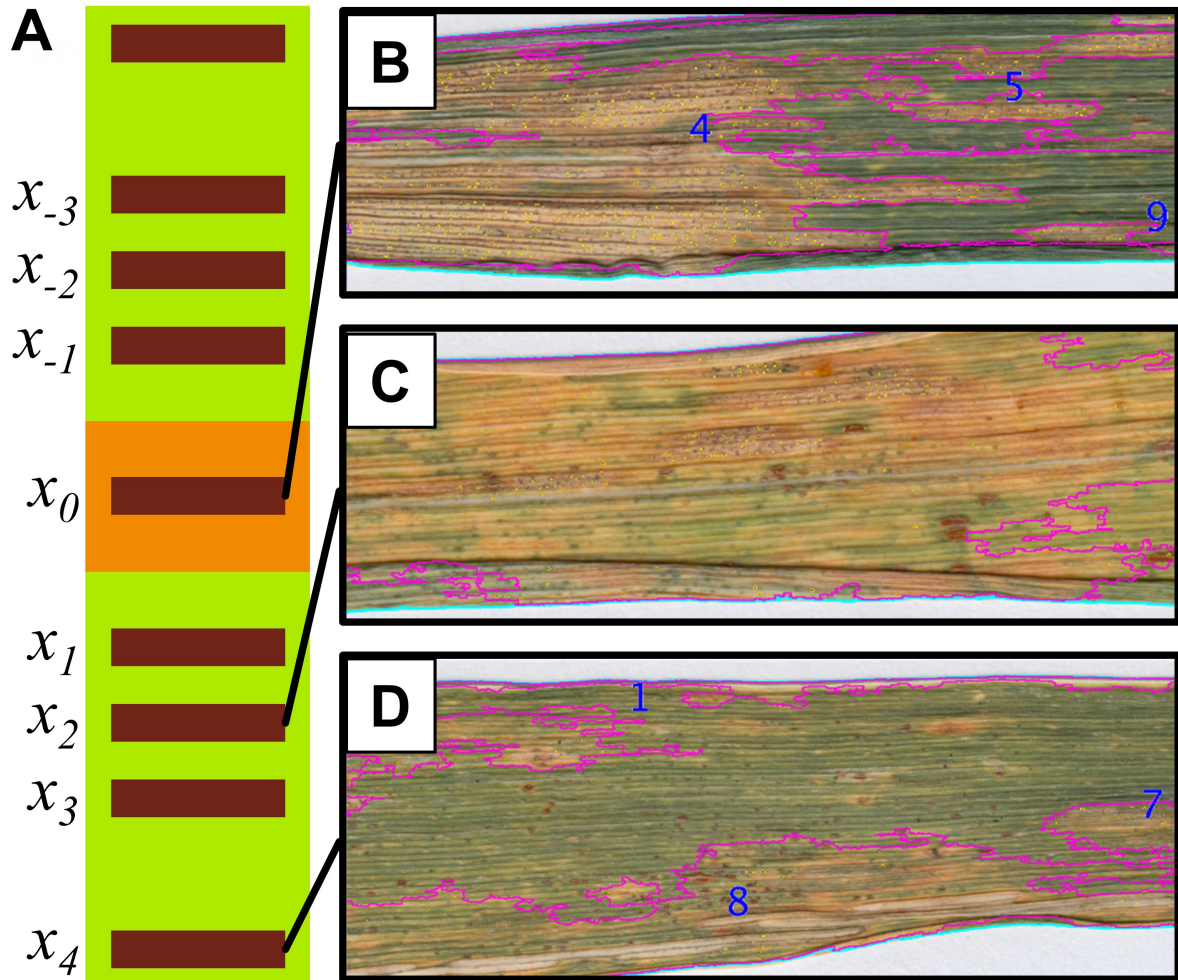


Figure 2: (A) Design of the experimental plot. 40 cm-wide inoculation area in the middle of the plot (orange). Distances from the middle of the inoculated area (x_0) to the middle of each measurement line were 0 cm, 40 cm, 60 cm, 80 cm, and 120 cm. (B, C, D) Overlay images illustrate the automated image analysis. Leaves collected from measurement lines x_0 (B), x_2 (C) and x_4 (D) of the treatment D at the sampling date t_1 . Cyan, purple and yellow lines mark borders of leaves, lesions and pycnidia, respectively.

where I_0 is the intensity (pycnidia/leaf) in the inoculation area at t_0 ; β is the transmission
214 rate (unitless) describing how many new pycnidia there will be produced in the measured
leaf layer per unit of measured intensity in the source leaves; $w = 112.5$ cm is plot
216 width; $b = 12.5$ cm is width of the border excluded from measurement lines; and α
is the dispersal parameter describing the dispersal kernel. The integration over the
218 measurement line divided by area of the line, $10(w - 2b)$, gives the average disease
intensity in a measurement line, representing uniform sampling of leaves.

220 Note that 10 cm width of measurement lines was practically the smallest possible
width that could be achieved in our field measurements, because the foliage of even a
222 single straw spans more than 10 cm, limiting the spatial resolution of our measurements.
For this reason, we simplified the model by neglecting the width of measurement lines
224 and assigning all disease intensity values recorded within each measurement line to
the distance from the source that corresponds to the middle of the line. With this
226 simplification, disease gradients were calculated according to

$$I_{t_1}(x^*) = \frac{I_0\beta}{w - 2b} \int_b^{w-b} \int_0^{40} \int_0^w \frac{e^{-\sqrt{(x^*-x_s)^2+(y_d-y_s)^2}/\alpha}}{2\pi\alpha^2} dx_s dy_s dy_d. \quad (7)$$

228 We compare results obtained using Eq. (6) and Eq. (7) to results obtained using sev-
eral simplifying assumptions. As implied by Madden et al. (2007) and the analysis of
230 Fitt et al. (1987), dispersal is often modeled as a one-dimensional process. However,
this simplification leads to correct estimates of the dispersal kernels only under certain
232 circumstances, as discussed above in Theory section. To test what kind of error we make
using the one-dimensional approach, we constructed the following function describing
234 the dispersal according to an exponential kernel in one dimension:

$$I_{t_1}(x^*) = I_0\beta \int_0^{l_s} \frac{e^{-r(x_s, x^*)/\alpha}}{2\alpha} dx_s. \quad (8)$$

236 Here the integral takes sum over the length of the source along the plot, $l_s = 40$ cm.

When measuring the gradient outside of the inoculation area, ($x \geq 40$ cm) the integral
238 can be solved analytically and the equation (8) is greatly simplified:

$$I_{t_1}(x^*) = \frac{I_0\beta}{2} (e^{l_s/\alpha} - 1) e^{-x^*/\alpha} \quad (9)$$

240 leading to the same structure as in the equation (2) (with $C = \frac{I_0\beta}{2} (e^{l_s/\alpha} - 1)$). Equation
(9) can be used directly to fit empirical disease gradients when considering the measure-
242 ment line as a point. When taking into account the real width of the measurement
line (10 cm) we calculate the mean intensity within a measurement line taking sum over
244 it and dividing by the width. Continuing from the equation (9) the gradient is now
calculated as

$$\begin{aligned} I_{t_1}(x^*) &= \frac{I_0\beta}{2} (e^{l_s/\alpha} - 1) \int_{x^*-5}^{x^*+5} \frac{e^{-x_r/\alpha}}{10} dx_r \\ &= \frac{I_0\beta\alpha}{20} (1 - e^{l_s/\alpha}) (e^{-5/\alpha} - e^{5/\alpha}) e^{-x^*/\alpha} \end{aligned} \quad (10)$$

which still retains the same form as the equation (2) but with a different constant than
248 in the equation (9) ($C = \frac{I_0\beta\alpha}{20} (1 - e^{l_s/\alpha}) (e^{-5/\alpha} - e^{5/\alpha})$). In this example, we retained
the same shape of the gradient despite adding the spatial extension of both the source
250 and the destination along the direction of the gradient. This highlights the memoryless
property of exponential kernels (Box 2).

252 We constructed the functions similar to the one in Eq.(8) also using the Gaussian
kernel and the power-law kernel (Box 1). These were compared to Eq.(9) based on
254 AIC-score (Akaike information criterion Akaike, 1973). The differences in the AIC-
scores were lower than the single parameter penalty, for this reason we conclude that
256 neither of the three kernels can be considered superior.

Estimation of dispersal and transmission parameters. The data we used in the
258 analysis were obtained in the following way. First, we collected incidence measurements

(counts) and acquired conditional severity measurements using image analysis. Second,
260 the severity data in each measurement line were multiplied with the corresponding in-
cidence to obtain unconditional severity measurements. Third, we calculated mean for
262 each measurement line to obtain five data points for each distance in each treatment.
These means over each measurement line were used for fitting. The dispersal gradient
264 functions (Eqs. (6), (7), (9), (10)) were fitted to the data to estimate α and $I_0\beta$.

To compare treatments and dispersal directions we used the bootstrapping approach.
266 We re-sampled our collected samples with replacement to create a large set of variable
bootstrap samples. Variation in the bootstrap samples reflects the variation that we
268 expect to observe if the actual experiment was repeated several times (see for example
Davison and Hinkley, 1997). Bootstrapping allowed us to model explicitly the variation
270 related to incidence counts and variation related to leaf collection, separately of each
other. This approach also allowed us to assess uncertainties in parameter estimates
272 without making any assumptions about the distributions of the data or the parameter
values.

274 We created 100 000 bootstrap samples for each measurement line. First, we re-sampled
the infected leaves, i.e. generated 100 000 new samples of original size sampling from
276 original leaf data with replacement. Second, we simulated the incidence counts on the
measurement lines to create a distribution of incidence values. Based on the measured
278 plant density (730 stems/m²) we had on average 82 leaves within a measurement line. In
this way, we simulated incidence counts with a population of 82 plants and all possible
280 incidence values (from 0/82 to 82/82) 100 000 times each and recorded the “real” inci-
dence value each time when the simulation gave the same incidence as in the observed
282 data. Third, the mean of each bootstrap set of leaf severity was multiplied by incidence
value drawn from the corresponding incidence distribution to obtain the unconditional
284 mean severity for each measurement line. Fourth, we grouped these unconditional means

of measurement lines into sets of five representing the five replicates. As a result, we
286 obtained 100 000 bootstrap replicates of the entire experiment.

The one-dimensional disease gradient in equation (9) was fitted to each of the 100 000
288 bootstrap replicates. Two-dimensional disease gradient function in equation (7) was
fitted to a subset of 10 000 bootstrap replicates. As a result, we obtained a large number
290 of bootstrap point estimates of parameters α and βI_0 for each treatment and direction.
These estimates were used to conduct statistical tests.

292 **Statistical tests.** Parameter differences were tested using a simple bootstrap hypoth-
esis test (Davison and Hinkley, 1997, p.162), where the observed difference between
294 parameter values in different conditions is compared to a distribution of differences ob-
tained with bootstrap samples. Significance level (p -value) of the test is calculated by
296 dividing the number of cases where the difference in the test statistic t_i is greater than
or equal to the observed difference t_{obs} by the number of bootstrap replicates (R) plus
298 the observed case:

$$p = \frac{1 + \#\{t_i \geq t_{obs}\}}{R + 1} \quad (11)$$

300 If only a few bootstrap samples give a more extreme difference than the observed one,
then the observed difference is considered significant. We tested the differences between
302 parameter estimates using Eq. (11).

Additionally, we tested differences between α - and βI_0 -estimates simultaneously using
304 a two-dimensional hypothesis test based on the joint distribution of differences in α and
 βI_0 (analogous to Johansson et al., 2014). A kernel density estimate of the joint distribu-
306 tion was obtained to define the degree of “extremity” of a point in the two-dimensional
parameter space. The point reflecting observed difference in the two parameters was
308 compared to the distribution of differences between bootstrap replicates. The observed
difference is considered significantly different from zero, if it is located in a sufficiently

310 sparse area, such that less than 5% of the bootstrap estimates are located in regions
with equal or lower density (the “equidensity test”).

312 We present 95% confidence intervals for the parameters derived from the distribution
of bootstrap results, i.e. the limits of 2.5th and 97.5th percentile of the distribution.

314 Differences in disease levels between treatments A, B and D were tested at t_0 , x_0 and
 t_1 , $x_{\pm 1}$ with the Kruskal-Wallis test and the pairwise Dunn’s posthoc comparison with
316 the Bonferroni correction.

Statistics implementation. All data analysis was implemented in Python (versions
318 3.5.2 and 3.6.0) and the code is provided together with the data. Fitting was performed
using lmfit-package (v. 0.9.10, Newville et al., 2014). Numerical integrations were im-
320 plemented with ‘quad’ and ‘dblquad’ functions in scipy-package (v. 1.0.1, Jones et al.,
2001–). Fitting of the two-dimensional functions (Eq. 6 and 7) was performed using
322 the high performance computing cluster Euler of the ETH Zurich. Kruskal-Wallis test
was conducted with ‘kruskal’ function in scipy-package and Dunn’s test with function
324 ‘posthoc_dunn’ in package scikit-posthocs (v. 0.3.8, Terpilowski, 2018).

Results and discussion of the experiment

326 The inoculations with *Z. tritici* strain 1A5 (treatment A), strain 3D7 (D) and their mix-
ture (B) were successful: at t_0 we observed increased disease levels in the inoculation
328 areas of all three treatments (Fig.3 A). Subsequently, disease gradients reflecting the
dispersal gradients were obtained. At t_1 , there was a gradient of disease severity from
330 higher levels at $x_{\pm 1}$ to lower levels at $x_{\pm 4}$ (Fig.3 B). Genotyping of re-isolated strains
confirmed the successful spread (Appendix C). In total, 4190 plants were inspected for
332 incidence counts; 2527 leaves were collected and analyzed using the digital image anal-
ysis. Total analyzed leaf area was 4.56 m² and the total number of observed pycnidia
334 was 1 131 608. The entire dataset including raw data, bootstrap replicates, best fit-

ting parameter estimates and weather data is available in DATADRYAD (TBA after
336 acceptance in the journal).

Pathogen dispersal

338 Fitting the equation (7) to the observed disease gradients allowed us to estimate pa-
rameters α (dispersal parameter) and βI_0 (transmission rate \times initial intensity at the
340 source). In treatment A, estimates of α were very low and estimates of βI_0 were very
high, compared to treatments B and D (Table 1). These unrealistic results (discussed
342 below) were likely due to an insufficient disease intensity within the inoculation area
and consequently a shallow gradient outside the inoculation area (Fig. 3 A and B). Less
344 successful pathogen spread in treatment A than in other treatments was confirmed by
comparing disease levels between treatments A and D at t_0 , x_0 and at t_1 , $x_{\pm 1}$. At t_0
346 x_0 , the disease intensity was significantly lower in treatment A than in treatment D
(Kruskal-Wallis test $p = 0.005$, pairwise Dunn's test $p = 0.004$). Further, at t_1 $x_{\pm 1}$
348 the intensity in treatment A was lower than the intensity in both treatments B and D
(Kruskal-Wallis $p = 3.4 \times 10^{-26}$; Dunn's test A vs B $p = 2.6 \times 10^{-18}$; Dunn's test A vs D
350 $p = 6.0 \times 10^{-24}$). For this reason, the next steps of analysis were conducted only using
data obtained in treatments B and D.

352 Comparison of the best-fitting parameters (Eq. (7), Table 1) between the positive
and the negative directions revealed no significant difference neither in treatment D
354 (equidensity p-value: $p_{2D} = 0.21$, one-dimensional hypothesis test Eq. (11) for parameter
 α : $p_\alpha = 0.17$, parameter βI_0 : $p_{\beta I_0} = 0.13$, Fig. 4 A), nor in treatment B ($p_{2D} = 0.74$,
356 $p_\alpha = 0.60$, $p_{\beta I_0} = 0.95$). This similarity between directions suggests isotropic dispersal.

As there was no significant difference between the two directions, we combined the
358 data from the two directions and estimated the parameters using the combined dataset.
We observed a significant difference between treatments B and D using the combined
360 dataset ($p_{2D} = 0.014$, $p_\alpha = 0.020$, $p_{\beta I_0} = 0.018$, Fig. 4 B). Dispersal parameter α was

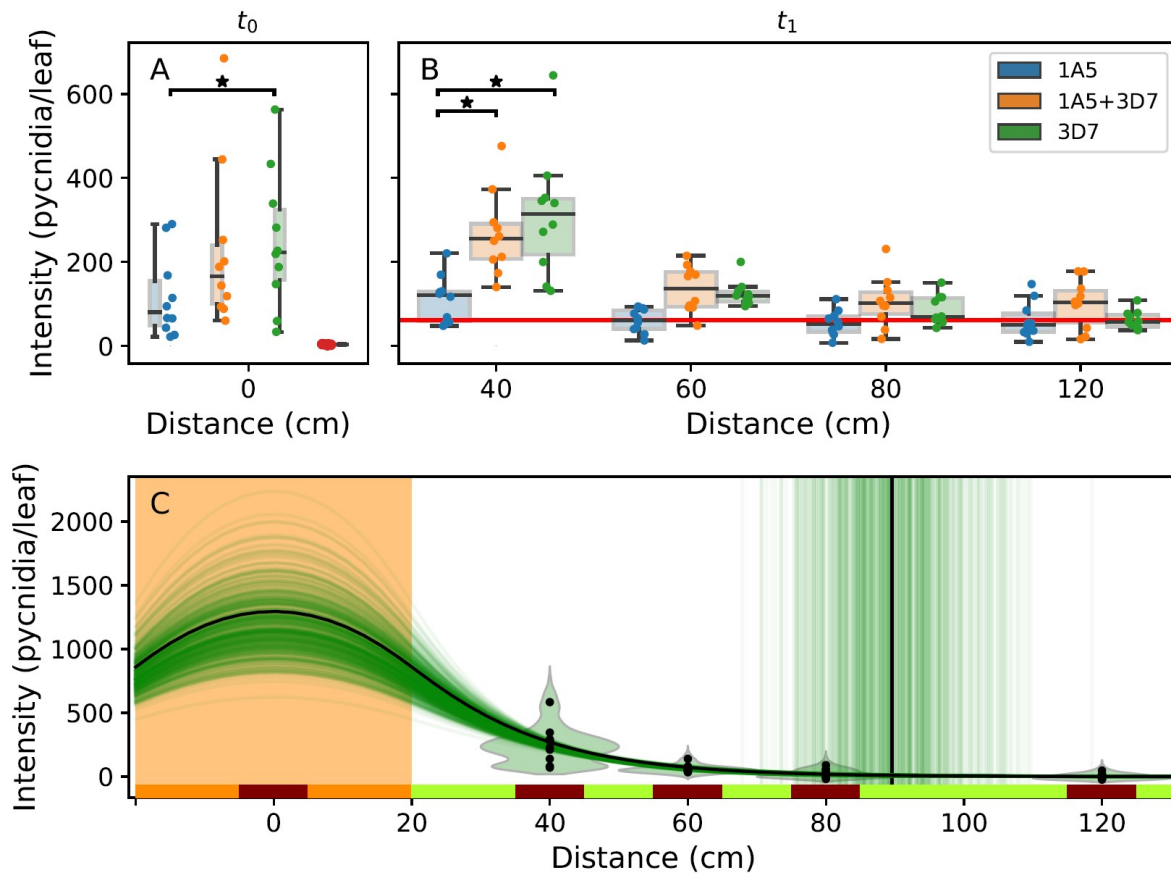


Figure 3: Disease levels and derived dispersal gradients. Data in blue shows treatment A (strain 1A5), in orange treatment B (mixture of 1A5+3D7), in green treatment D (strain 3D7), and in red treatment C (control). A: Disease levels in the inoculation area at t_0 . Means of replicates shown with dots. Layers F and F-1 shown for treatments A, B, and C; while layer F-2 for treatment C (no disease on F-1 nor F). B: Disease gradients at t_1 after the spread event. Blue, orange and green dots and boxes show F leaf data. Red lines: mean over control plots. Black horizontal bars with asterisks show significant pairwise differences between treatments at t_0 and at t_1 (40 cm). C: Disease gradients of treatment D, using Eq. (9). Black dots show the observed replicate means (same as green dots in (B)) and black curve shows the best fitting gradient function. Vertical black line shows 99th percentile of the dispersal distance (Eq. (A3): x_{99}). Distributions of bootstrap data, disease gradients, and x_{99} values of 500 bootstrap replicates shown in green violin plots, curves and horizontal lines, respectively.

higher in treatment B while βI_0 was higher in treatment D (Table 1). Thus the mixture
 362 of the two strains dispersed further, but imposed lower infection pressure on host plants
 than the strain 3D7 alone. Estimated values $\alpha_D = 13.5$ cm and $\alpha_B = 21.4$ cm fall close to
 364 the range estimated in spore dispersal experiments with artificial rain (Fitt et al., 1987).
 The one-dimensional estimates of α (Table 2) correspond to half-distances 10.5 cm (strain
 366 3D7) and 17.0 cm (strain mixture), which match well to the range of 6–16 cm reported
 by Fitt et al. (1987). We conclude that experiments in controlled conditions translate
 368 well to the field conditions, at least when using simplistic one-dimensional fitting. The
 dispersal occurred due to two short rain showers (Fig. B2). During a longer rainy period
 370 the spores may disperse in multiple splash events leading to longer average dispersal
 distances and flatter disease gradients (Fitt et al., 1989).

Table 1: Best fitting parameters from fitting Eq. (7).

Treatment	-direction	α (95% CI), cm	βI_0 (95% CI), pycnidia/leaf
A	-positive	2.5	99992
	-negative	4.9	3518
	-combined	2.6	99975
B	-positive	23.1 (15.9 - 37.5)	1271 (1052 - 1618)
	-negative	20.0 (14.8 - 28.4)	1281 (1049 - 1586)
	-combined	21.4 (16.7 - 28.6)	1271 (1095 - 1468)
D	-positive	15.3 (12.3 - 19.7)	1559 (1147 - 2112)
	-negative	12.0 (9.3 - 15.5)	2387 (1613 - 3638)
	-combined	13.5 (11.5 - 16.1)	1915 (1475 - 2430)

Note: Confidence intervals (CI) derived from bootstrapping, but not for biologically implausible results of treatment A. Values of βI_0 were limited below 100 000.

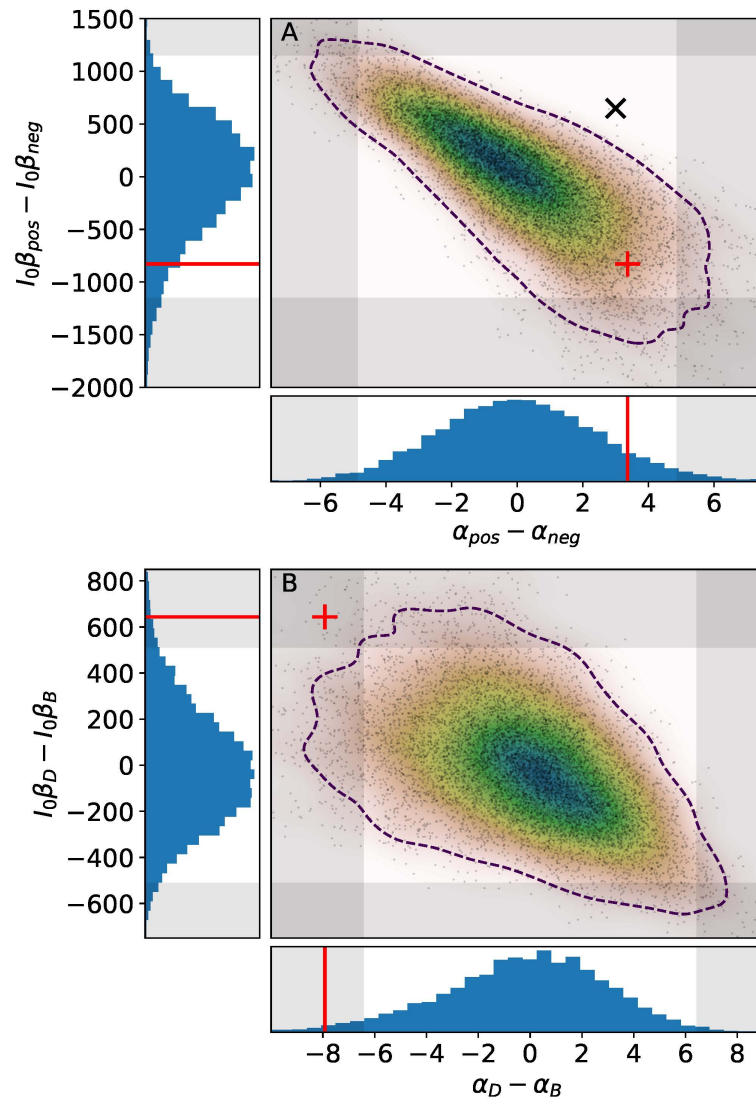


Figure 4: Visualization of one- and two-dimensional bootstrap tests, in histograms and main panels, respectively. (A) Comparison between two directions in treatment D. (B) Comparison between treatments D and B. Histograms show single parameter distributions while heat maps and black dots show joint distributions (10 000 replicates). Observations (red line; red plus) in the 5% extreme of the distribution (shaded area; outside of the dashed line), are considered significant. The differences are significant between treatments (B) but not between directions (A). Black cross in panel (A) shows a hypothetical observation where the difference would be deemed non-significant for each parameter separately (non-shaded area), but the joint test reveals a significant difference (outside of the dashed line).

372 Disease transmission

Besides the dispersal parameter, we were also able to estimate transmission rate of the
374 disease. The fitting yielded estimates of βI_0 , from which we extracted β by dividing βI_0
by estimates of I_0 . We estimated $I_{0,B} = 227$ pycnidia/leaf and $I_{0,D} = 249$ pycnidia/leaf.
376 Based on those we calculated $\beta_D = 7.7$ (unitless) and $\beta_B = 5.6$. Estimation of β was
only possible because we defined the scale parameter in a biologically meaningful
378 manner.

Parameter estimates for the strain 1A5 were not realistic. It is not biologically plau-
380 sible that spores of the strain 1A5 would disperse by only 2-5 cm, while spores of the
strain 3D7 spread some 14 cm, because pycnidiospores of the two different strains are
382 expected to have the same physical properties. Likewise, the transmission rate estimates
of 1A5 were unrealistically high (Table 1). However, we inferred the parameter βI_0 for
384 the strain 1A5 assuming that the physical process of spore transport via rain droplets
is the same for the two strains. Under this assumption ($\alpha_A = \alpha_D = 13.5$ cm), we found
386 that the dispersal of the strain 1A5 was isotropic ($p = 0.38$). Furthermore, with the two
directions combined, we estimated $\beta I_0 = 349$ pycnidia/leaf and $\beta = 3.0$ for treatment A
388 ($I_{0,A} = 118$ pycnidia/leaf).

The transmission rates of strain 1A5 and the strain mixture were lower than that of
390 strain 3D7 (1A5 vs 3D7: $p = 1.00 \times 10^{-4}$, mixture vs 3D7: $p = 0.0498$). The intermediate
transmission of the strain mixture is likely the result of a combination of transmission
392 rates of the two strains. Strain 1A5 is known to produce fewer and smaller pycnidia
than strain 3D7 on cultivar Runal in greenhouse (Stewart et al., 2018). Our results in
394 field conditions are consistent with previous findings, as 1A5 produced fewer pycnidia
within the source area (Fig. 3 A) and had a lower estimate of the transmission rate.

396 In this study system, the infectivity depends on weather conditions (Henze et al.,
2007). Also, the disease levels within the source source and along the disease gradient

398 were measured only on highest leaves, but dispersal occurred likely to and possibly from
the lower leaf layers, which were not included in our analysis. Hence, the reported
400 transmission rates should be considered relative to each other rather than as absolute
values.

402 Genotyping

In total, 153 individuals of *Z. tritici* were isolated from separate pycnidia on the leaves
404 collected from the experimental plots and genotyped using targeted PCR-primers (Ap-
pendix C). The genotyping of the re-isolated strains supported the conclusions drawn
406 from the phenotypic data. (i) The strains spread out from the source area; we detected
them on the measurement lines (9 isolates out of 19 were detected as strain 1A5 at $x_{\pm 1}$
408 on treatment A, 45/55 as 3D7 on treatment D). (ii) There was a decreasing disease
gradient; proportion of putative 1A5 and 3D7 isolates was lower further away from the
410 inoculation area (2 + 37 (1A5 + 3D7) out of 49 isolates at $x_{\pm 1}$ vs 1 + 8/30 at $x_{\pm 3}$, on
treatment B). (iii) The strain 1A5 was transmitted less successfully than 3D7; propor-
412 tion of the putative 3D7 strain individuals in treatment D was higher than proportion
of 1A5 individuals in treatment A (see (i)) and the same effect was visible in treatment
414 B (see (ii)). Thus, the genotypic and phenotypic data were in agreement.

How good are the simplifications?

416 Simplifying the analysis of dispersal data by reducing the source and the destination
to one dimension or even to points allows for simpler and faster calculation than in
418 the two-dimensional analysis. However, these simplifications may lead to less accurate
estimates of parameters. We compare the simplifications used based on (i) accuracy of
420 the estimates, (ii) effect on statistical tests, and (iii) computational time.

(i) The values of parameter α were higher in one- than in two-dimensional approach
422 (Table 2). If one would use the parameter estimates derived with one-dimensional ap-

proach (as found in literature) in a two-dimensional model, the dispersal would be over-
424 estimated as the values of α tend to be higher. This overestimation relates to the general
“flattening” of disease gradients from extended sources. Compared to a point source, an
426 extended source contributes to the gradient mostly through the tail of the dispersal ker-
nel, which tends to be more flat than the beginning of the kernel. When an extended
428 source is considered as a point, the flattening effect of the source geometry is accounted
for in larger estimates of the width of the kernel.

430 On the other hand, the relationship between the population spread and dispersal pa-
rameter α is different between one- and two-dimensional models. This difference becomes
432 clear for example when dispersal is described based on “mean dispersal distance” which
is α for one-dimensional exponential kernel but 2α for two-dimensional. In treatment
434 D, the corresponding mean dispersal distances are $2\alpha_{2D} = 27$ cm and $\alpha_{1D} = 15$ cm -
a considerable difference. Clearly, a one-dimensional model of dispersal should not be
436 used for deriving dispersal distances on a population level. One should also be careful
not to confuse the half-distance of an exponential dispersal location kernel with median
438 dispersal distance of the population (see Appendix A).

(ii) All the statistical tests based on the bootstrap replicates gave similarly significant
440 or non-significant results for one-dimensional and two-dimensional parameter estimates.

(iii) Regarding the computational time, one-dimensional fitting of the disease gradient
442 based on Eq. 9 to 100 000 bootstrap replicates was easily performed on a PC in a
few hours, while fitting the two-dimensional function (Eq. 7) required a few days of
444 computational time for only 10 000 replicates. When using the most complex function
with two area integrals [Eq.(6)] it took more than 12 hours on a PC to obtain the
446 estimates for only the observed data with one replicate.

Table 2: Comparison of parameter estimates between different functions.

Equation	Treatment B		Treatment D	
	α , cm	βI_0 , pycn./leaf	α , cm	βI_0 , pycn./leaf
Eq. 6, 2D extended destination	21.4	1265	13.5	1889
Eq. 7, 2D line destination	21.4	1271	13.5	1915
Eq. 10, 1D extended destination	24.6	1123	15.1	1994
Eq. 9, 1D point destination	24.6	1131	15.1	2031

Note: Estimates from using the combined data of the two directions. “2D” and “1D” stand for two- and one-dimensional models, respectively.

Discussion

448 We propose an approach for estimating dispersal kernel parameters, where the source
geometry is explicitly incorporated in the model. This provides a solution for correcting
450 inaccurate estimates caused by unjustified simplifying assumptions (See Fig. 1 and Table
2). This approach also provides a quantitative answer to the question “By how much
452 and in which way does the source geometry affect the observed dispersal gradient?”,
instead of more qualitative statements regarding the “flattening” of the gradient with
454 a larger source (Zadoks and Schein, 1979; Ferrandino, 1996; Cousens and Rawlinson,
2001). Using our method, we are able to relax the requirement of having a point source
456 in a dispersal experiment. This helps designing experiments by increasing the power
of the source and consequently the amount of collected data, which may be a limiting
458 factor in many systems. With our approach, one can use results acquired from different
experimental designs (e.g. those cited in Fitt et al., 1987) to estimate dispersal kernels
460 in each case. Those can then be compared to each other directly, in contrast to dispersal
gradients that reflect differences in experimental designs and cannot be compared if the
462 designs are different. Most importantly, our approach allows to estimate actual kernel
parameters in a much wider range of empirical studies than it was recognized previously,
464 that includes all studies with spatially extended sources. In this way, “we can move from
descriptions of pattern to a grasp of process” (Bullock et al., 2006).

466 We show, with simulations (Fig. 1) that different source geometries may lead to similar
gradients when the kernel is either memoryless or separable. However, most kernels
468 are neither memoryless nor separable, and thus distortions of the gradient shape are
expected with varying source geometry. In any case, such simulations can be used when
470 planning an experiment to guide the experimental design and to test predicted outcomes.
Simulated outcomes of an experiment can also help to determine when the source can be
472 considered a point and what kind of errors this simplification may introduce. Clearly, our
two-dimensional models of dispersal are simplifications of the three-dimensional process
474 (e.g. Vidal et al., 2018). If the third dimension is of great importance, as perhaps in
aquatic environments or with tree canopies (Cousens and Rawlinson, 2001), modeling of
476 source geometry and dispersal processes in three dimensions may be necessary.

We used this approach to analyze the data we acquired on *Z. tritici*, showing how
478 different simplifying assumptions lead to different results. The explicit consideration of
source geometry allowed us not only to estimate kernel parameter α but also a biolog-
480 ically relevant transmission rate β , instead of a meaningless normalization factor. Our
experiment was conducted using an artificial experimental design with passively dispers-
482 ing organisms, but similar approach can be used in observational studies in nature and
with actively dispersing organisms whenever the source area can be characterized and
484 the dispersal process can be described with the help of dispersal kernels.

In the common case of anisotropic dispersal (Soubeyrand et al., 2007), the validity
486 of the simplifications based on separability or memorylessness of the specific functional
forms of kernels, will generally not hold. However, the more general integration method
488 that we presented can be modified to take into account the anisotropy of the kernel.
In the modified model, the probability of dispersal from a source point to a destination
490 point should depend not only on the distance between the points, as in our case, but
also on the direction from the source to the destination. In this way, also anisotropic

492 dispersal kernels can be inferred from measurements of dispersal gradients with the
explicit consideration of the source geometry.

494 Our theoretical analysis shows that most pronounced differences between the dispersal
gradients originating from different source geometries appear close to the source, while
496 at larger distances from the source these differences disappear (Fig. 1B, C, D). The
effect is seen in each of the three very different types of kernels, indicating that it is
498 a universal feature. Therefore, even when the size of the source is much smaller than
the gradient length, it could be that the size of the source is still comparable to the
500 characteristic dispersal distance (i.e., the distance over which the dispersal kernel changes
substantially). In this case, measurements close to the source will be substantially
502 distorted due to the finite area of the source. Therefore, simple rules of thumb stating
that to be considered as a point, the size of the source should be smaller than 1% of the
504 length of the gradient (Zadoks and Schein, 1979; McCartney et al., 2006), can be quite
misleading, and result in inaccurate estimates of dispersal parameters. This emphasizes
506 the importance of explicit modeling of the source geometry as we have done it here,
considering that it is often the case that most measurements are conducted close to the
508 source even when the overall gradient is long (Werth et al., 2006; Skarpaas and Shea,
2007; Loebach and Anderson, 2018).

510 Experiments that measure dispersal are difficult and laborious (Bullock et al., 2017).
Geometry of the source, location of sampling areas, amount of sampling at different
512 locations and other components of the experimental design may have a large effect on
the precision and generalizability of the results. We support Skarpaas et al. (2005)
514 calling for optimization of dispersal study designs by simulations, to make the most out
of the effort.

516 Acknowledgements

PK and AM gratefully acknowledge financial support from the Swiss National Science
518 Foundation through the Ambizione grant PZ00P3_161453. Genetic Diversity Centre at
ETH Zurich helped with the genetic analysis. PK and AM would like to thank Andreas
520 Hund and Hansueli Zellweger for maintenance of the field experiment. FS would like to
thank Christophe Montagnier, Sandrine Gélisse and Nicolas Lecutier for maintenance
522 of the similar field experiment prepared at the facilities of INRA Bioger in Thiverval-
Grignon, France.

524 Appendix A: Dispersal distance kernel

Dispersal distance kernel. Dispersal kernels are not only used to describe distribu-
526 tions of locations of dispersed individuals, but also to summarize dispersal distances,
such as mean distance travelled. Dispersal distance kernel is a one-dimensional func-
528 tion describing the probability of individuals to end up at a certain distance from the
source. It can be derived from a two-dimensional dispersal location kernel by integrat-
530 ing it around the source, essentially by multiplying it with $2\pi r$ (Nathan et al., 2012).
The shape of the dispersal location kernel can differ substantially from the shape of the
532 dispersal distance kernel (e.g. Cousens and Rawlinson, 2001; Nathan et al., 2012). The
dispersal distance kernel corresponding to exponential dispersal location kernel is given
534 by

$$\kappa_{e,dist}(r) = 2\pi r \frac{e^{-r/\alpha}}{(2\pi\alpha^2)} = \frac{r e^{-r/\alpha}}{\alpha^2} = \frac{r^{k-1} e^{-r/\alpha}}{\alpha^k \Gamma(k)}, \quad k = 2, \quad (\text{A1})$$

536 where $\Gamma(2) = 1$ is the gamma function. Equation (A1) gives the one-dimensional gamma-
distribution with the shape parameter $k = 2$ and the scale parameter α .

538 It is important to keep in mind that means and medians of dispersal location kernels
do not generally correspond to means and medians of population dispersal distances
540 (i.e. means and medians of dispersal distance kernels). The example of the exponential
kernel is of particular importance, as this kernel is often described with the half-distance.
542 Considering the one-dimensional exponential kernel, the dispersal parameter α gives the
mean and $\alpha \ln(2)$ (half-distance) gives the median of the distribution. However, in the
544 case of the two-dimensional exponential location kernel the mean dispersal distance is
not α but 2α (i.e. mean of the gamma-distribution in Eq. (A1)). Furthermore, median,
546 or any percentile, of the dispersal distance distribution can be determined by solving the
equation

$$548 \int_0^{x_L} \kappa_{e,dist}(r) dr = 0.01L \quad (\text{A2})$$

where x_L is the L^{th} percentile of dispersal distance ($L \in [0, 100]$). After integration, the
550 Eq. (A2) reads

$$e^{-x_L/\alpha} \left(1 + \frac{x_L}{\alpha}\right) = 1 - 0.01L. \quad (\text{A3})$$

552 We solve Eq. (A3) numerically to obtain the median dispersal distance $x_{50} \approx 1.7\alpha \gg$
 $0.69\alpha \approx \ln(2)\alpha$. Considering the limits of population dispersal, Golan and Pringle
554 (2017) defined 99th percentile of the dispersal distance distribution as a limit for the
long-distance dispersal in fungi. At $L = 99$, we find $x_{99} \approx 6.6\alpha$. These numbers have
556 applied relevance, for example in conservation biology or in precision agriculture when a
treatment is targeted to a certain fraction of a dispersing population. Mean or median
558 dispersal distances or other characteristic numbers should be determined using the two-
dimensional location kernel and the corresponding distance kernel.

560 The limit of long-distance dispersal (x_{99} , Eq. (A3)) corresponding to observed values
of α is 90 cm for treatment D and 142 cm for treatment B. In an agricultural field, a visible
562 disease focus (Zadoks and van den Bosch, 1994) and significant host damage (Shaw and
Royle, 1993) would occur close to the source due to higher density, while the edge of the
564 population is likely to incur less damage because of lower pathogen density. This hidden
pathogen population in the tails of the distribution should be taken into account when
566 attempting spatially targeted treatments, for example in precision agriculture involving
focal fungicide spraying.

568 Appendix B: Field experiment

The study system

570 *Zymoseptoria tritici* (formerly *Mycosphaerella graminicola*) is a major fungal pathogen of
wheat in temperate areas (Jørgensen et al., 2014; Dean et al., 2012). It causes the disease
572 *Septoria tritici* blotch (STB), which is visible as brownish lesions on wheat leaves. The
lesions reduce the photosynthetic ability of the host and cause yield losses of 5-10%, even
574 when resistant cultivars and fungicides are used in combination. Annually in Europe
some 1.2 billion dollars are spent for fungicides mainly aimed to control STB (Torriani
576 et al., 2015).

Infection by *Z. tritici* begins when spores deposited on wheat leaves germinate and
578 penetrate the leaves through stomata (Kema et al., 1996). The fungus grows in the
apoplast for several days without visible symptoms (Duncan and Howard, 2000). In
580 optimal conditions, necrotic lesions appear in the invaded host tissue after about ten days
and asexual fruiting bodies called pycnidia begin to form (Kema et al., 1996; Duncan
582 and Howard, 2000). Asexual pycnidiospores ooze from pycnidia within water-soluble
cirri and are spread mostly by rain splash. If a spore falls within the wheat canopy and
584 stays on a healthy leaf instead of being washed down, it can infect new host tissue either
on the same or on the neighbouring plants. Upon successful infection, the spore again
586 creates a lesion and produces new pycnidia within the lesion. The pathogen undergoes
several rounds of asexual reproduction per growing season. Zhan et al. (1998, 2000)
588 estimated that $\approx 66\%$ of infections on flag leaves came from asexual spores, leading to
conclusion that asexual reproduction is the most important source of infection on flag
590 leaves.

Initial inoculum by air-borne ascospores is often considered uniform across a wheat
592 field and not a limiting factor for epidemics (Morais et al., 2016). Therefore, much of

interest has been on vertical dispersal of the spores from initial infection of seedlings to
594 emerging leaf layers (Shaw, 1987; Lovell et al., 1997; Bannon and Cooke, 1998; Lovell
et al., 2004; Vidal et al., 2018). Interaction between the pathogen and the host has been
596 described by Robert et al. (2018) as a race, where the pathogen need to “climb” up to
the next leaf layer before current layer becomes senescent and its resources are depleted.
598 The plant, in turn, “tries” to save the newly emerging leaves making them escape the
infection by fast stem elongation.

600 However, horizontal dispersal greatly influences the ability of a particular clonal lin-
eage to grow in numbers and can play a major role in the dynamics of emerging fungicide
602 resistance or ability to overcome host resistance genes. Resistance gene pyramids or ho-
mogeneous host cultivar mixtures may select for multiple virulences in a single pathogen
604 strain. Thus, spatial adjustment of control strategies has been suggested as a potentially
more sustainable solution and optimal spatial scale of such heterogeneity is determined
606 by the spatial scale of the pathogen’s horizontal spread (Mundt and Browning, 1985;
Brophy and Mundt, 1991; Newton et al., 2009; Sapoukhina et al., 2010; Newton and
608 Guy, 2011; Djidjou-Demasse et al., 2017). Dispersal of *Z. tritici* or similarly spread-
ing species *Parastagonospora nodorum* (formerly *Septoria nodorum*) has been studied
610 in controlled conditions using either infected straw or spore suspension together with
artificial rain and often spore traps (Brennan et al., 1985; Saint-Jean et al., 2004; Vidal
612 et al., 2017). Bannon and Cooke (1998) studied the effect of wheat-clover intercrop on
dispersal from plates via artificial rain and merely noted a reduction of dispersed spores
614 at the 15 cm distance. No experiment has so far been conducted in field conditions to
estimate parameters of dispersal kernel of the disease spread from infected plants to the
616 surrounding healthy canopy.

Spatial spread directly influences the number of new hosts that a pathogen can poten-
618 tially invade and it also affects the spatial distribution of the pathogen population. For a

polycyclic pathogen, such as *Zymoseptoria tritici*, small differences in monocyclic spread
620 can result in considerable differences in the epidemic outcomes after multiple disease cy-
cles. Thus, understanding the mechanisms and the scale of the spread will improve our
622 ability to predict and control potentially disastrous epidemics of the disease.

Plant materials and agronomic practices

624 The experiment was performed at the Field Phenotyping Platform (FIP) site of Eschikon
Field Station of the ETH Zurich, Switzerland (Kirchgessner et al., 2017). Experimental
626 plots were sown with winter wheat (*Triticum aestivum*) cultivar Runal on 1 November
2016. Sowing density was 440 seeds/m² and the observed stem density on 19 June 2017
628 was 730 stems/m². Field maintenance included herbicide Herold SC (0.6 l/ha; Bayer)
on 2 November 2016, and stem shortener Moddus (0.5 l/ha; Syngenta) on 13 April 2017.
630 Fungicide Input (1.25 l/ha; Spiroxamin 300 g/l, Prothioconazol 160 g/l; Bayer) was
applied on 13 March 2017 to suppress the background infection.

632 Similar experiment was prepared also at the facilities of INRA Bioger in Thiverval-
Grignon, France (coordinates: 48.840N, 1.952E). The experimental design was similar
634 with minor modifications. Due to uncondusive weather conditions the inoculation failed
to produce measurable primary disease gradients. Therefore, the data is not presented.

636 Experimental design

The experimental plots were 1.125 m × 4 m rectangles consisting of nine long rows of
638 wheat with 12.5 cm spacing between the rows. Plots were randomly assigned to four
treatments with five replicates of each treatment as shown in Fig. B1. The four treat-
640 ments were: inoculation with strain ST99CH_1A5 (short identifier 1A5, treatment A),
strain ST99CH_3D7 (3D7, treatment D), both strains (B) and no inoculation (C).
642 Strains were collected in Switzerland in 1999 as described by Zhan et al. (2002) (see also

www.septoria-tritici-blotch.net/isolate-collections.html).

644 In each plot, there was a 40 cm-wide inoculated area across the plot in the middle.
Disease measurements were conducted in the middle of the inoculated area ($x_0 = 0$ cm)
646 and at eight locations outside of the inoculated area, four on each side at distances
 $x_{\pm 1} = \pm 40$ cm, $x_{\pm 2} = \pm 60$ cm, $x_{\pm 3} = \pm 80$ cm and $x_{\pm 4} = \pm 120$ cm from the center of
648 the inoculated area (see Fig. 2 A). A measurement line consisted of a line across the
experimental plot at the given distance, extended with 5 cm margins along the plot and
650 excluding 12.5 cm borders at the edge of the plot to reduce edge effects. Measurements
were conducted uniformly over space in the rectangular area of each measurement line.

652 *Z. tritici* inoculation

Inoculum was prepared by growing the fungus for seven days in yeast-sucrose-broth
654 (<https://dx.doi.org/10.17504/protocols.io.mctc2wn>). The liquid culture was then fil-
tered, spores were pelleted in centrifuge and re-suspended into sterile water to harvest
656 blastospores. The washed spore suspension was diluted to achieve the concentration of
 10^6 spores/ml. For treatment B the final spore concentration was 10^6 spores/ml so that
658 each strain was present with the concentration of 5×10^5 spores/ml. Finally, we added
0.1 % (v/v) of Tween20 and kept the inoculum suspension on ice until spraying.

660 Inoculation was performed by spraying 300 ml of the spore suspension onto the inoc-
ulation site of each plot using a hand-pump pressure sprayer. The plots were inoculated
662 during the late afternoon to avoid direct sunlight. All treatments were inoculated with

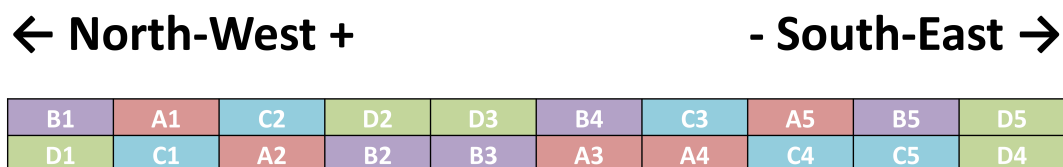


Figure B1: Arrangement of the plots in the field.

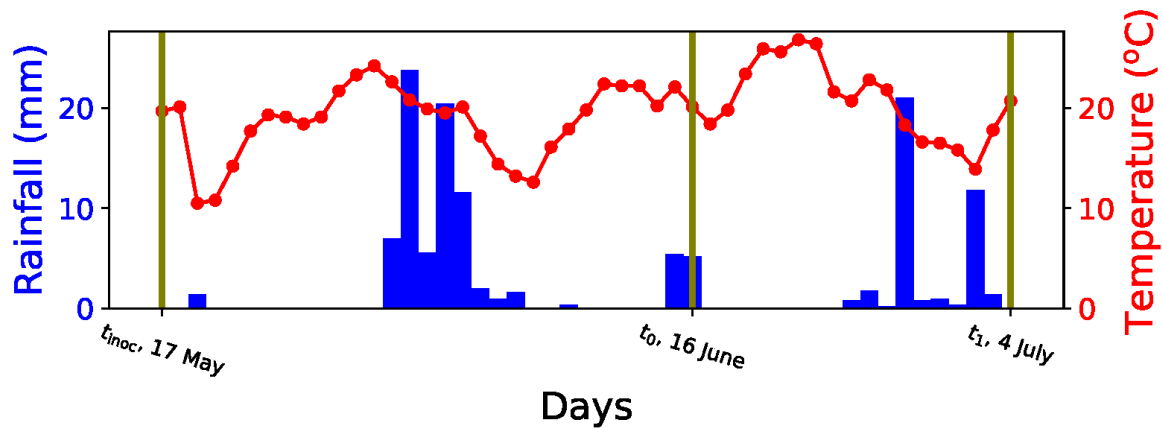


Figure B2: Weather conditions during the experiment. Daily precipitation in the blue bars, daily mean temperature in the red line, dates of inoculation, sampling dates t_0 and t_1 are shown using vertical lines.

the same sprayer, which was rinsed with water and 70% ethanol to clean all parts before
664 inoculating each treatment. Entire canopy within the inoculation area was inoculated
until runoff. During spraying, the inoculation area was bordered with plastic sheets to
666 avoid the spillover of the inoculum to other plots. After spraying, the border sheets were
folded over the canopy to enclose the plants in plastic tents maintaining high humidity
668 overnight. The tents were removed early next morning to avoid overheating of plants.
The inoculation was repeated next evening in the same manner. Pictures of inoculation
670 are shown in Appendix D.

First attempt to inoculate was made on 5 and 6 April, when F-3 layer (the third leaf
672 layer below flag leaf) was mostly emerged (approximate growth stage, GS 22, Zadoks
et al. (1974)), and inoculation success was assessed on 24 April and again on 3 May.
674 Due to cold weather the inoculation success was extremely low: we observed low levels
of disease in the F-3 leaf layer and the plants were in the beginning of stem elongation
676 (F-1 emerging, GS 35). Average incidence in F-3 layer in the inoculated area 3 May was
6.1%, 2.9%, 0% and 4.9% for treatments A, B, C, and D, respectively. We considered the
678 inoculation as failed, because the secondary spread from such low initial infection levels

would likely cause only negligible gradients and due to stem elongation and senescence
680 the highest leaf layers would likely escape the spread (Robert et al., 2018). We decided to
inoculate again the higher leaf layers to achieve stronger, measurable disease gradients.
682 Dates of this main inoculation were 17 and 18 May 2017, when flag leaves had already
emerged (GS 39–41).

684 **Assessment of the disease gradient**

The disease assessment combining incidence and severity measurements was performed
686 twice. At t_0 , on 14 June 2017 (GS 70) only the inoculation areas were assessed to
confirm the success of inoculation across the measurement line x_0 . Flag leaves outside
688 the inoculation area were visually confirmed to be healthy without further assessment.
At t_1 on 4 July 2017 (GS 85) all measurement lines of treatments A, B and D were
690 sampled. One line on each plot of treatment C was assessed for reference.

At t_0 , incidence of the disease was measured at the leaf scale in the following manner.
692 Thirty to forty straws were inspected on each measurement line. The highest diseased
leaf layer was recorded for each straw. The leaves lower than that were assumed to
694 be diseased as STB is usually more prevalent in the lower leaf layers. Additionally,
naturally senescent leaf layers were recorded. In this way, incidence was estimated for
696 all non-senescent leaf layers. After estimating the incidence, eight infected leaves were
collected from up to two consecutive leaf layers that had incidence higher than 20%. The
698 collected leaves were then mounted on paper sheets and scanned with 1200 dpi resolution.
The resulting images were analyzed using automated image analysis method measuring
700 two aspects of severity of the infection that represent the host damage and pathogen
reproduction, as described in Karisto et al. (2018). Host damage was measured as the
702 percentage of leaf area covered by lesions (PLACL) and pathogen reproduction as the
pycnidia count per leaf. The sampled leaf layers at t_0 were the flag leaf layer (F) and

704 the layer below it (F-1).

At t_1 , the plants were already mostly chlorotic and hence the incidence measurement
706 was not possible in the field. Instead, we collected about 24 leaves from each mea-
surement line at random. The leaves were taken into lab and each leaf was visually
708 inspected for the presence of pycnidia. Incidence was recorded based on the presence of
pycnidia on the collected leaves and only leaves with pycnidia were scanned for severity
710 measurement. Due to vast chlorosis, the measurement of host damage was considered
unreliable and only pathogen reproduction was used in the subsequent analysis. Thus,
712 we measured the disease intensity as numbers of pycnidia per leaf.

We estimated number of asexual reproduction and dispersal events between t_0 and
714 t_1 using the following arguments. First, based on the data from Shaw (1990) regarding
latent period lengths of *Z. tritici* at different temperatures (as revisited in Karisto et al.
716 (2018), Fig. A1), latent period after inoculation was approximated to be longer than 20
days (average daily temperature during first 19 days was 19°C). Thus, there was likely
718 no spread from inoculation area during the rainy period at 13–17 days after inoculation
(dai) (Fig. 2). This was confirmed with visual assessments of the inoculation areas on
720 8 June (22 dai), when we observed few tiny lesions and mostly no pycnidia, concluding
that substantial spread had not been possible by then. Second, at t_0 (28 dai) there was
722 substantial disease (Fig. 3 A) in the inoculation areas and there were two strong showers
in the night after t_0 . Third, there was no rain for one week before nor after t_0 . Thus, we
724 conclude that there was most likely only one asexual spread event at t_0 , which caused
the disease gradients outside of the inoculation areas at t_1 (38 dai).

726 In summary, the inoculation was successful and led to increased levels of disease in the
inoculation areas after a latent period of 3–4 weeks, at t_0 . Three weeks later, at t_1 there
728 were clearly visible symptoms outside of the inoculation area. The observed symptoms
at t_1 can be entirely accounted to the raining event and consequent asexual spread of

730 the pathogen at t_0 .

Discussion of experimental aspects

732 **Measurement of pathogen population, not host damage.** Our estimates of dispersal kernel correspond to the effective dispersal of the pathogen population, instead of
734 the basic dispersal kernel of all spores. Difference between these may arise from possibly density-dependent post-dispersal mortality (Nathan et al., 2012; Klein et al., 2013). At
736 high spore densities, that can be found close to the source, leaves can become saturated with the infection leading to a decreased infection efficiency of spores (Karisto et al.,
738 2019). In the tail of the distribution the density is however so low, that saturation may not be a major factor. Dispersal of spores could be measured with spore traps placed
740 within the canopy. However, that would leave open how many of the spores actually attach to healthy plants, how many of them are successful, and how much the established
742 population disperses. Using healthy plants as spore traps leads to the measurement of a more epidemiologically relevant combination of dispersal and infection processes.

744 Measurement of pathogen reproduction in terms of numbers of pycnidia per leaf gives us a proxy of the pathogen population size at each measurement point. Traditionally,
746 plant diseases are observed visually based on host damage, but novel methodology allows for a different approach. While host damage is an important agronomic factor, pathogen
748 reproduction is more relevant for pathogen ecology and evolution. Moreover, pathogen reproduction is more powerful than host damage for predicting the host damage at a
750 later time point (Karisto et al., 2018).

Sampling distances. The measurement lines were at closest 20 cm (± 5 cm) from the
752 edge of the inoculated area. Measuring the gradient closer to the source and even inside the source could make the fitting more accurate, because differences between gradients
754 would be easier to detect closer to the source area where variations are more pronounced.

However, closer to the source, the reliability of data might suffer from saturation and
756 also from dispersal via direct contact (Fitt et al., 1989). Optimal measurement distances
have to be determined for each study system based on biological understanding and prior
758 knowledge about the dispersal kernel.

We measured the disease also inside the inoculation area, but those were excluded
760 from fitting to include only secondary infections. The increase in the disease intensity at
 x_0 from t_0 to t_1 was not only due to secondary infections but also from extremely long
762 latent periods (Karisto et al., 2019). Additionally, possible saturation was strongest at
 x_0 . Therefore, measurement of newly spread infection was not possible inside the source
764 area.

Appendix C: Genotypic test with PCR

766 **Primer design.** We designed four primer pairs targeted at each of the two strains. The
primers were aimed to be first fully specific for the target isolates 1A5 and 3D7 within
768 the set of four commonly used lab strains 1A5, 1E4, 3D1, 3D7 and second as specific
to the target strain as possible in the field. Specificity here means that the primers
770 designed for 1A5 should produce an amplicon in PCR only with 1A5 genome and not
with other strains. Strain specific primers would allow for a convenient detection of the
772 focal sub-population after the experiment as in a mark-recapture experiment.

To design the primers, we used presence-absence data of predicted genes from Hart-
774 mann and Croll (2017). We chose target regions that were present in the target strain
(either 1A5 or 3D7) and absent in the other three isolates (1E4, 3D1, and either 3D7
776 or 1A5). From those potential targets, we selected ten least frequent regions in the 27
Swiss isolates analyzed by Hartmann and Croll (2017). After selecting the target re-
778 gions, we designed four primer pairs that would be suitable for high throughput qPCR
in same conditions: amplicon length 100-150 bp, melting temperature around 60 °C. The
780 primers were designed to amplify regions in different chromosomes of the target strain
to minimize the possibility of finding all of them in a single strain in the field. Details
782 of the designed primers are given in Table C1.

Validation of primer specificity. First validation of the primers was done with qPCR
784 among the four strains 3D7, 1A5, 3D1 and 1E4 (Tables C2 and C3, Figures C1 and C2).
Successful amplification of the target DNA and no amplification on non-target DNA
786 suggested that each of the eight primer pairs was specific to their target strain among
the four strains, indicating successful primer design based on the genomes.

788 Primers' specificity was then validated in a natural population using multiplex-PCR
(Table C4, Table C5) combining each specific primer pair with a primer pair that is

Table C1: Primers

Primer	Sequence (5'-3')	T_m (°C)	Amplicon (bp)
1A5.5_FWD	AGC AGT CCT CGT AGC ATA ACG	59.93	135
1A5.5_REV	GAC CTC CTA TGA TGC GGC AA	59.89	
1A5.6_FWD	GGG AGG CCC TGG TTG ATT AC	60.11	135
1A5.6_REV	CTT GTA AGA GCG AGG GGC AA	60.04	
1A5.9_FWD	TTC TCT CTA TAG CCC GCC CT	59.52	137
1A5.9_REV	GAG TAG ACT CTA GAG GAA ACC TAG T	58.11	
1A5.10_FWD	CTC GGC CAG GAA GTG ATT GT	60.04	137
1A5.10_REV	GAG CAG TGG AGC CCA AGA AT	60.03	
3D7.2_FWD	CGA CAT CGG TTC AGA GAT GGA A	60.16	146
3D7.2_REV	GTA CCT TCG ATT CGT GCG GT	60.46	
3D7.6_FWD	CTT GGG TGC AAT GAA CGG AC	59.76	139
3D7.6_REV	TGA GAA ACA GTC GTG TGG CA	59.82	
3D7.9_FWD	CAG CTC GAC TTG TGA GTC CT	59.4	136
3D7.9_REV	CGT GCA AAC GCT GCA TGA T	60.15	
3D7.10_FWD	GGT GCC CTC GTC GGA ATA C	60.23	123
3D7.10_REV	TTG GGG AAG GAG ACC ATT CG	59.38	
Zt_gen_FWD	ATT GGC GAG AGG GAT GAA GG	60.5	101
Zt_gen_REV	ATT TTC GTG TCC CAG TGC GTG TA	60.5	

Note: Primer name starts with the target strain followed by chromosome number, except for Zt_gen primers. The latter designed by Duvivier et al. (2013).

Table C2: qPCR reaction mix, 20 μ l

Reagent	Concentration	Volume (μ l)	Final concentration
Water		6	
EvaGreen Mix	5X	4	1X
Strain.Chr_FWD	1 μ M	2	200nM
Strain.Chr_REV	1 μ M	2	200nM
Target DNA	1ng/ μ l	6	6ng/20 μ l

Note: We used qPCR mixture HOT FIREPol EvaGreen qPCR Mix Plus (ROX) (Solis BioDyne).

790 specific to *Z. tritici* generally (Zt_gen primers) (Duvivier et al., 2013). Zt_gen provided
a positive control for success of the PCR: if it created an amplicon, the reaction was
792 successful. Primers were tested against 37 natural strains isolated from the control plots
of the experiment. Reaction with primers 1A5.9 did not work reliably, indicated by the
794 lack of Zt_gen amplicon. Numbers of false positives for other primer pairs were 4, 8, 20,

Table C3: qPCR reaction cycles

Step	Temperature (°C)	Time (s)
1	95	900
2	95	15
3	60	20
4	72	20

Note: Steps 2–4 repeated 40 times

Table C4: PCR reaction mix, 20 μ l

Reagent	Concentration	Volume (μ l)	Final concentration
Water		6.34	
KAPA Buffer	2X	10	1X
Zt_gen_FWD	10 μ M	0.5	250nM
Zt_gen_REV	10 μ M	0.5	250nM
Strain.Chr_FWD	5 μ M	1	250nM
Strain.Chr_REV	5 μ M	1	250nM
KAPA3G Polymerase	2.5U/ μ l	0.16	2U/100 μ l
Spore solution	10 ⁴ -10 ⁶ sp/ml	2	

Note KAPA3G Plant PCR Kit (Kapa Biosystems).

Table C5: PCR reaction cycles

Step	Temperature (°C)	Time (s)
1	96	180
2	95	20
3	60	15
4	72	15
5	72	30

Note: Steps 2–4 repeated 35 times.

13, 12, 7 and 6 for 1A5.5, 1A5.6, 1A5.10, 3D7.2, 3D7.6, 3D7.9 and 3D7.10 respectively
 796 (Figures C3, C4, C5, C6, C7, C8, C9, C10). Importantly, none of the false positives of
 1A5.5 and 1A5.6 overlapped with each other, hence using combined data of those two
 798 gave no false positives. The six false positives of 3D7.10 were amplified with all the
 other 3D7-primers and none of the 1A5 primers. Thus, it is possible that they were the
 800 actual strain 3D7 either left on the field from previous years of field experiments or it

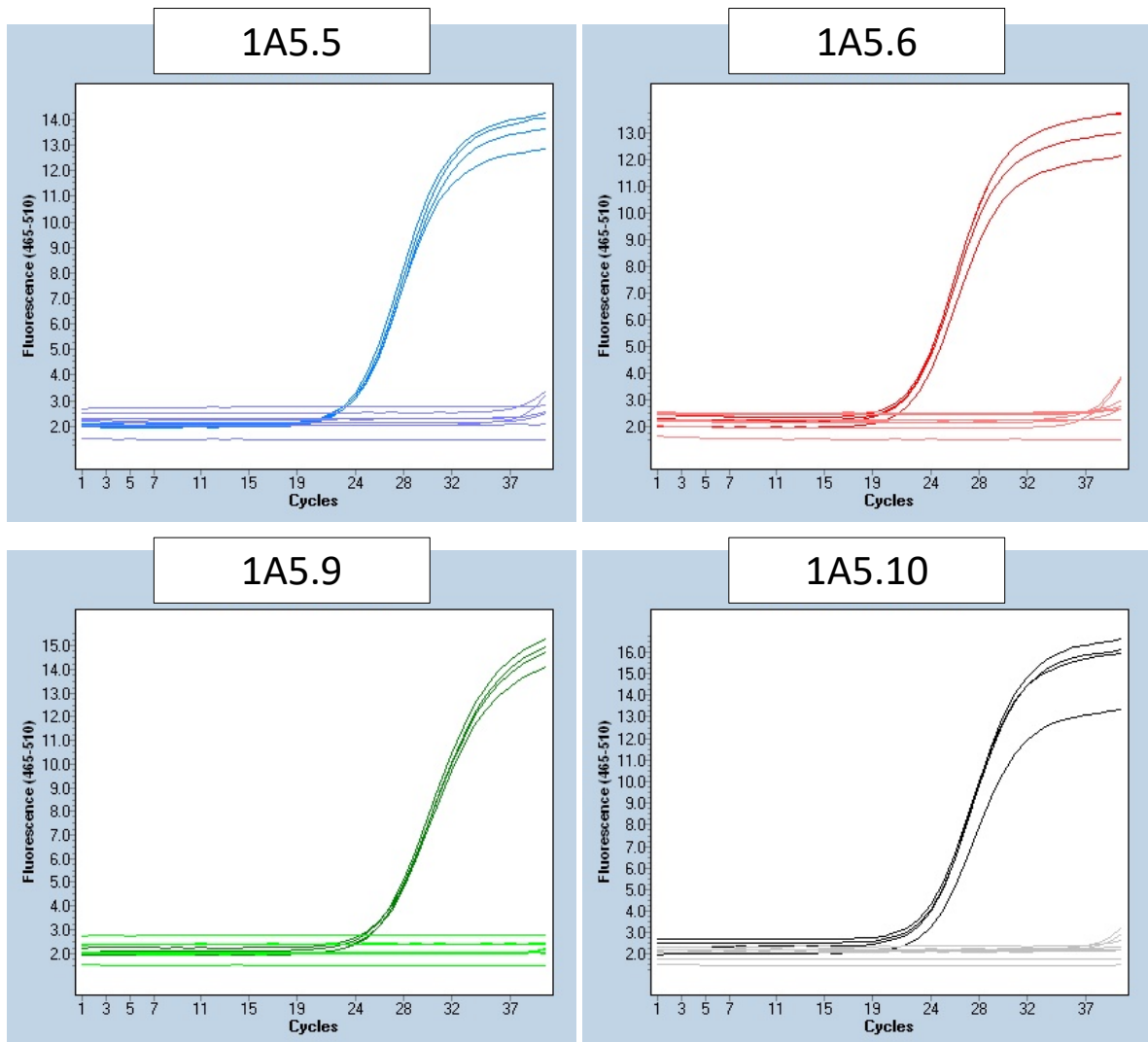


Figure C1: Amplification plots of the 1A5 targeting primers in qPCR. The amplified curves represent four replicates of 1A5, while the lower curves represent two replicates of each of 1E4, 3D1, 3D7 and water.

was a spill-over from the current treatments.

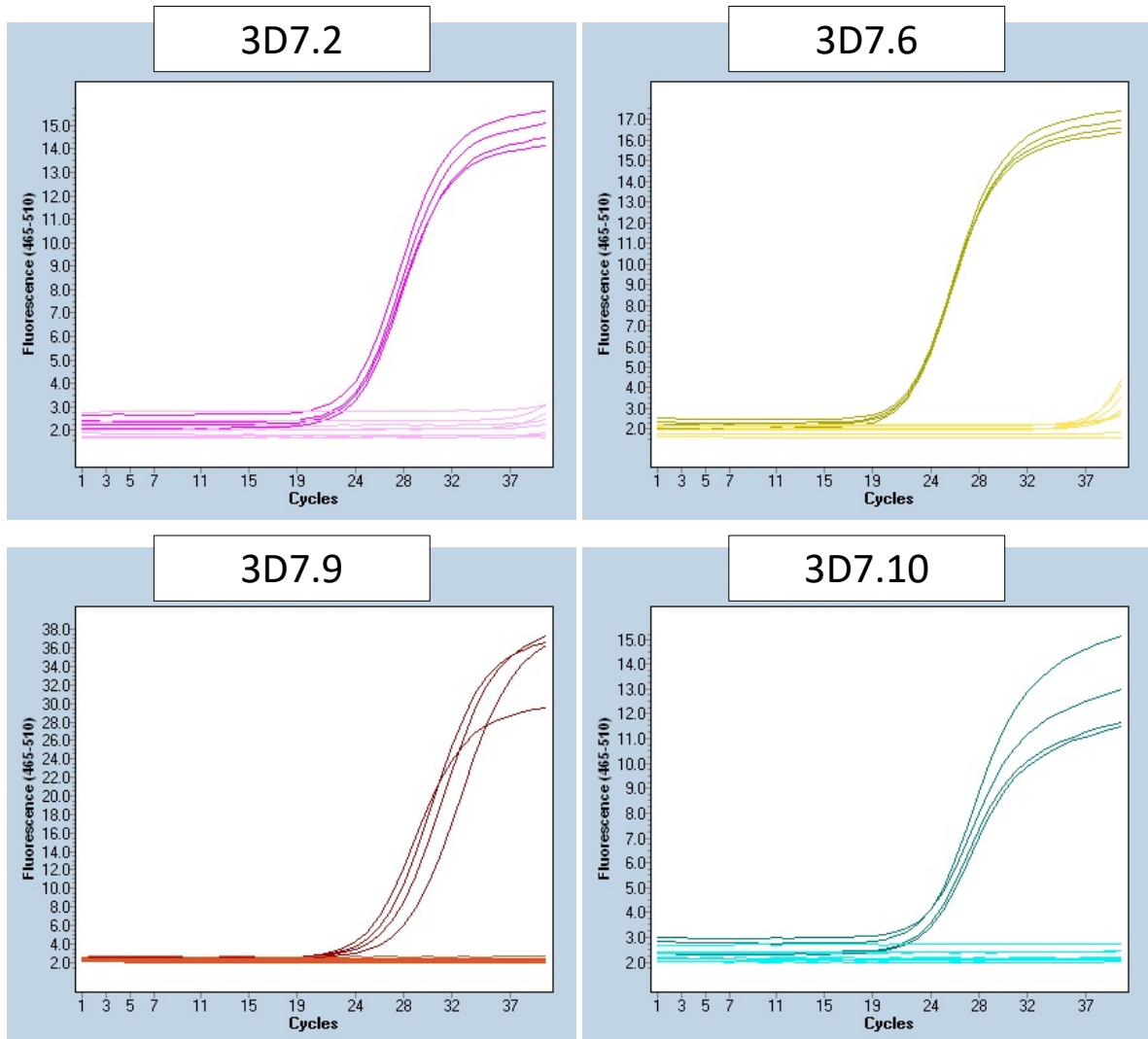


Figure C2: Amplification plots of the 3D7 targeting primers in qPCR. The amplified curves represent four replicates of 3D7, while the lower curves represent two replicates of each of 1A5, 1E4, 3D1 and water.

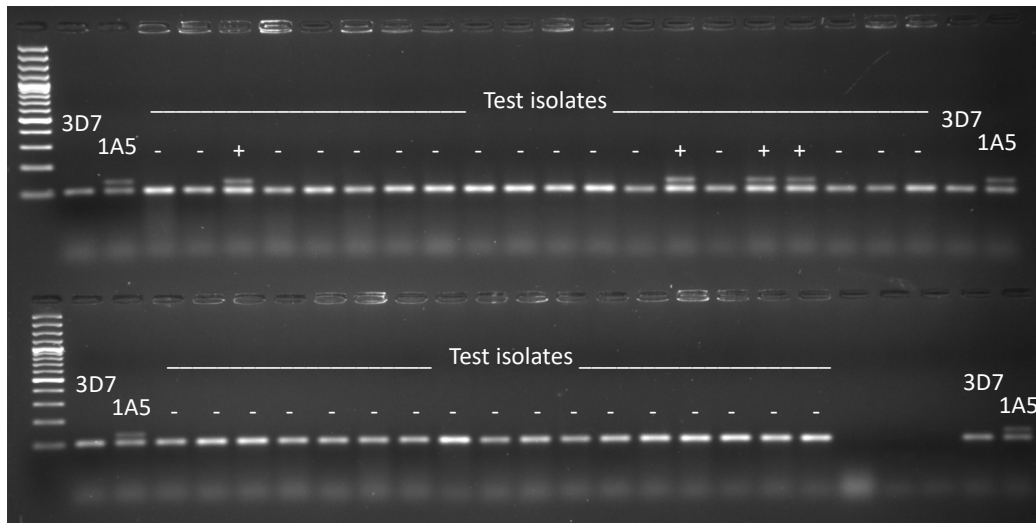


Figure C3: Amplicons from Zt_gen (shorter) and 1A5.5 (longer). Isolate 1A5 as positive control and 3D7 as negative control. Plus and minus indicate successful reaction (Zt_gen amplicon) and presence or absence of target amplicon, respectively.

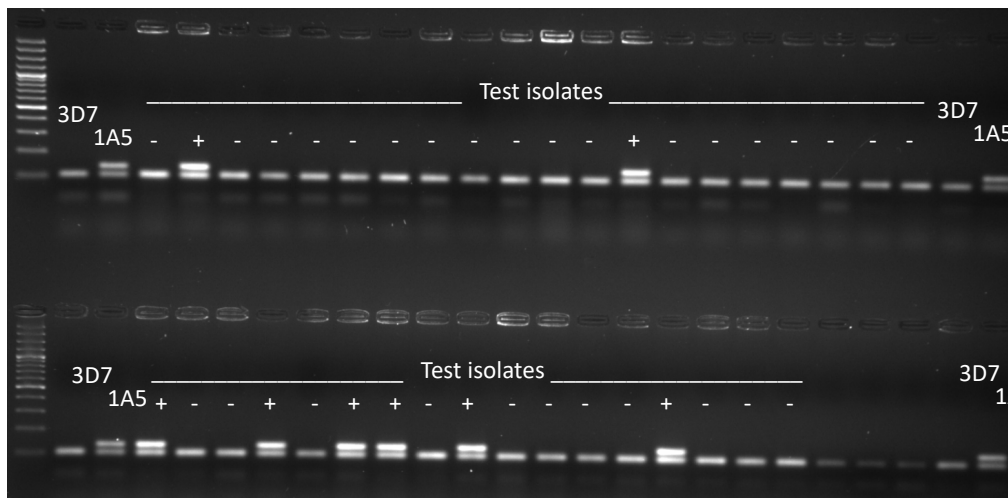


Figure C4: Amplicons from Zt_gen (shorter) and 1A5.6 (longer). Isolate 1A5 as positive control and 3D7 as negative control. Plus and minus indicate successful reaction (Zt_gen amplicon) and presence or absence of target amplicon, respectively.

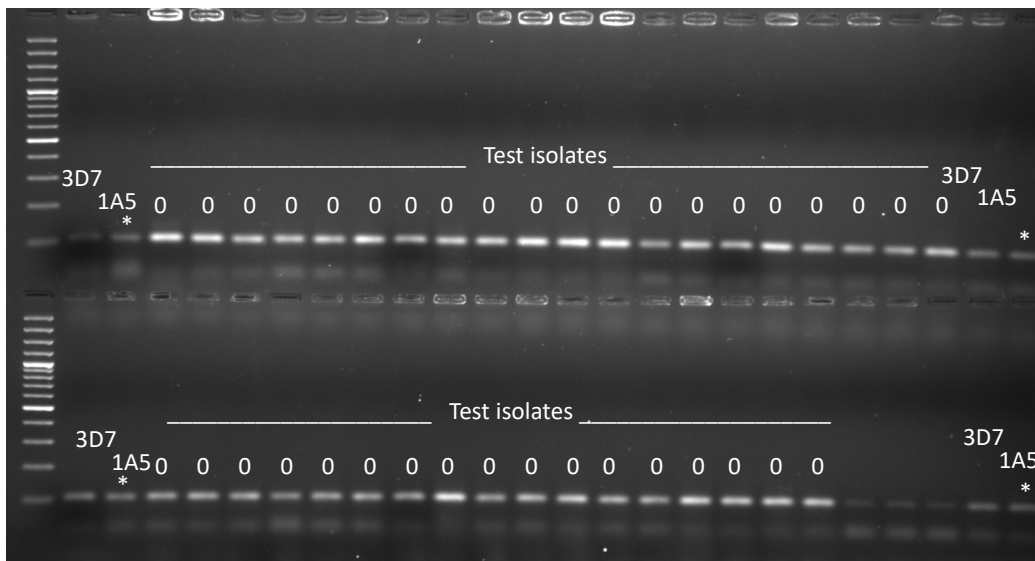


Figure C5: Amplicons from Zt_gen (shorter) and 1A5.9 (longer, not present). Isolate 1A5 as positive control and 3D7 as negative control. Zeros indicate that no conclusions were drawn from the reactions, as the positive controls were not amplified (*).

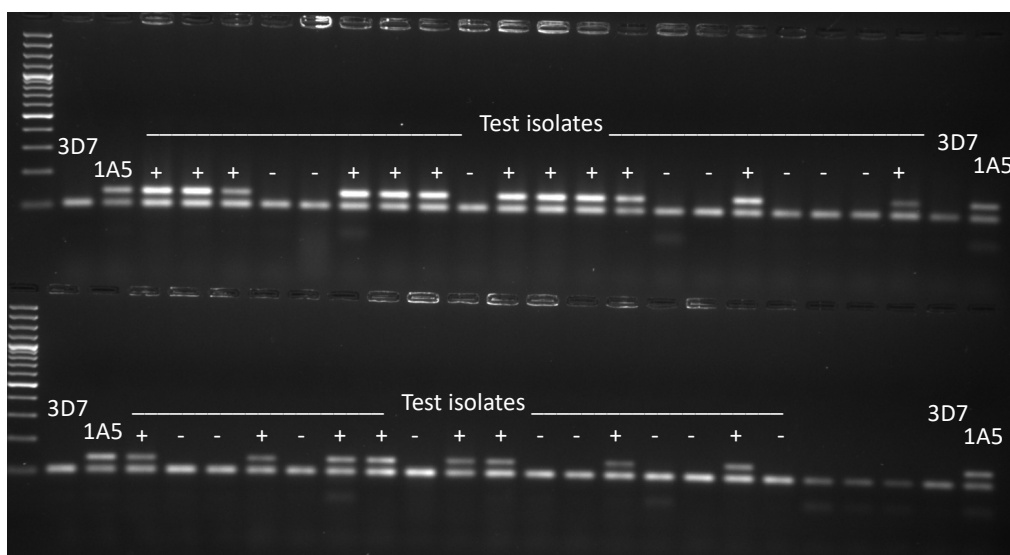


Figure C6: Amplicons from Zt_gen (shorter) and 1A5.10 (longer). Isolate 1A5 as positive control and 3D7 as negative control. Plus and minus indicate successful reaction (Zt_gen amplicon) and presence or absence of target amplicon, respectively.

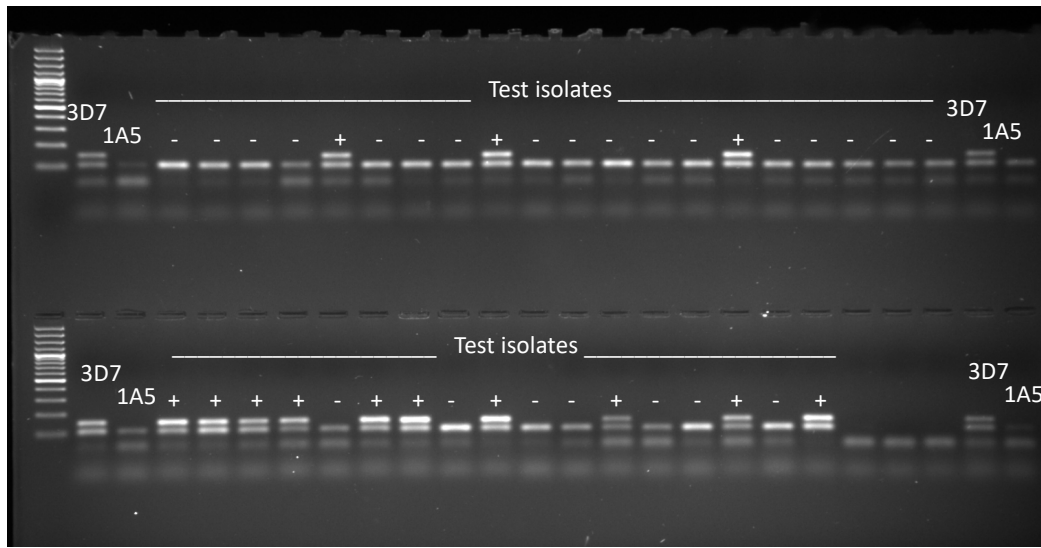


Figure C7: Amplicons from Zt_gen (shorter) and 3D7.2 (longer). Isolate 3D7 as positive control and 1A5 as negative control. Plus and minus indicate successful reaction (Zt_gen amplicon) and presence or absence of target amplicon, respectively.

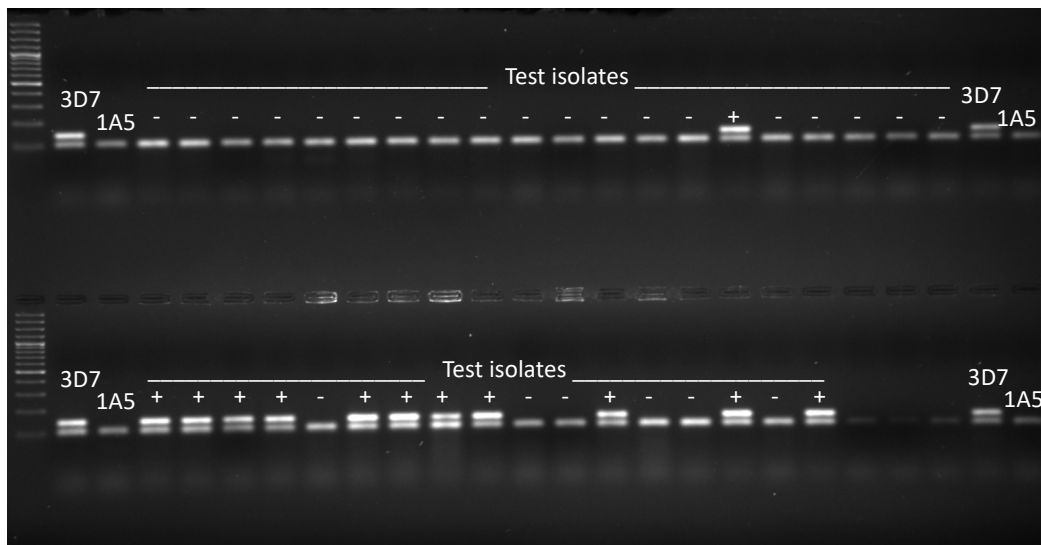


Figure C8: Amplicons from Zt_gen (shorter) and 3D7.6 (longer). Isolate 3D7 as positive control and 1A5 as negative control. Plus and minus indicate successful reaction (Zt_gen amplicon) and presence or absence of target amplicon, respectively.

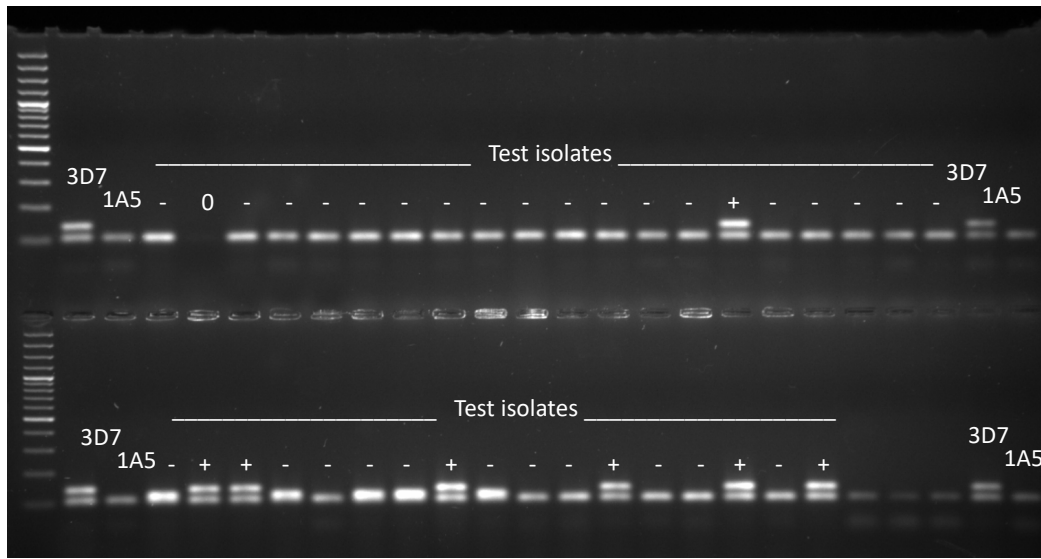


Figure C9: Amplicons from Zt_gen (shorter) and 3D7.9 (longer). Isolate 3D7 as positive control and 1A5 as negative control. Plus and minus indicate successful reaction (Zt_gen amplicon) and presence or absence of target amplicon, respectively.

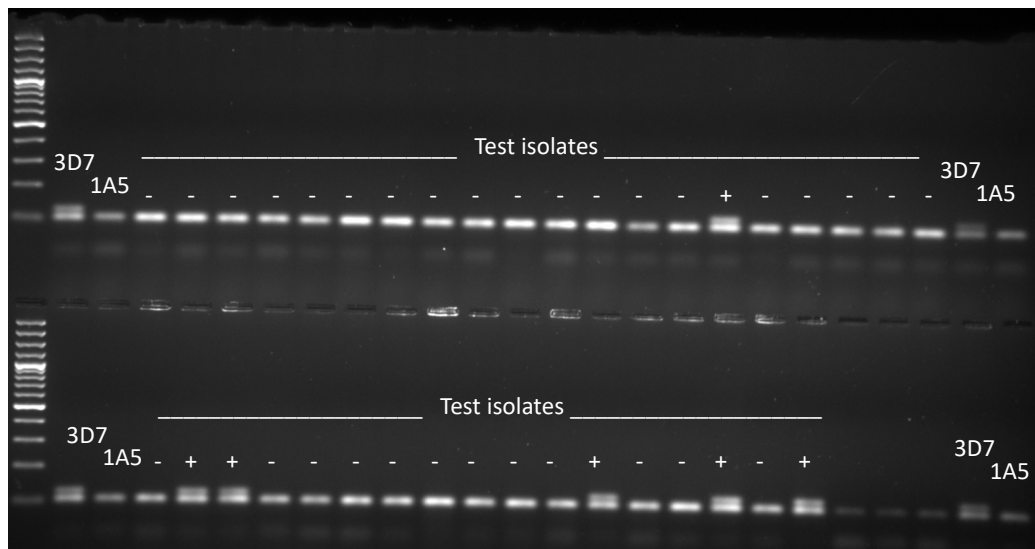


Figure C10: Amplicons from Zt_gen (shorter) and 3D7.10 (longer). Isolate 3D7 as positive control and 1A5 as negative control. Plus and minus indicate successful reaction (Zt_gen amplicon) and presence or absence of target amplicon, respectively.

802 **Genotyping of the re-isolated strains.** After validation, the primers 1A5.5, 1A5.6,
3D7.9 and 3D7.10 were chosen for genotyping the strains isolated from experimental
804 material. If both of the two primer pairs targeting either 3D7 or 1A5 showed amplifica-
tion, we called that a detection. On control plots, 6/37 strains tested were detected as
806 3D7 (16% false positives) while 0/37 strains were detected as 1A5 (0% false positives).
On a plot of treatment A (replicate 1), 9/19 strains (47%) at $x_{\pm 1}$ were detected as 1A5
808 (Fig. C11). In contrast, on a plot of treatment D (replicate 1), 45/55 strains (82%) at
 $x_{\pm 1}$ were detected as 3D7 (Figs. C12, C13). Thus, frequency of 3D7 was higher than
810 1A5 outside the inoculation area, as implied by the disease gradients (Fig. 3B). On a
plot of treatment B (replicate 1), at $x_{\pm 1}$ 2/49 were 1A5 and 37/49 were 3D7 while $x_{\pm 3}$
812 1/30 was 1A5 and 8/30 were 3D7 (Figs. C14, C15 for 1A5, and Figs. C16, C17 for
3D7). As expected, the proportion of the target strains decreased with distance. Lower
814 proportion of 1A5 is likely a result of two-fold effect of weaker transmission: first, the
strain produced fewer pycnidia in the inoculation area (treatment B, replicate 1, at x_0
816 t_0 : 1A5 4/15, 3D7 10/15, Figs. C11, C12, C13) and second, those pycnidia multiplied
themselves with lower success.

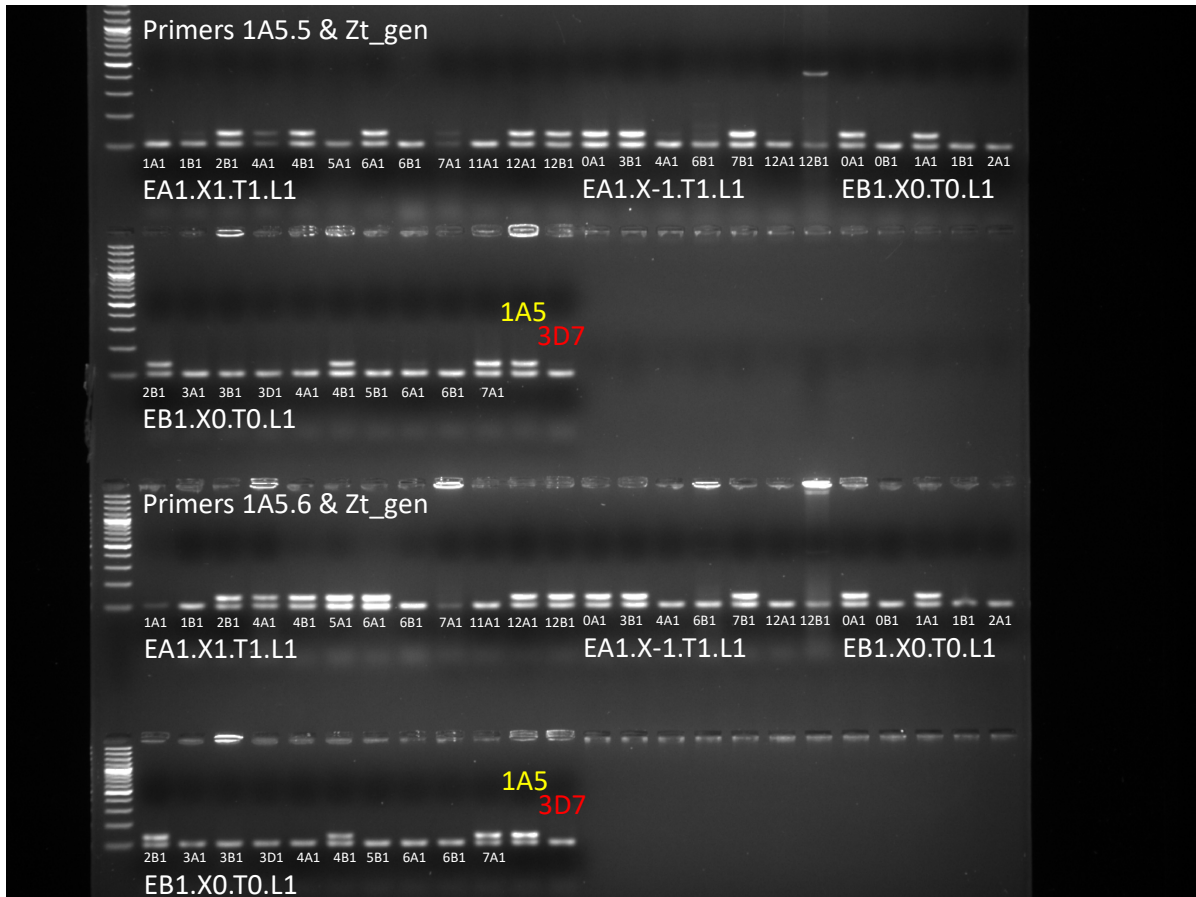


Figure C11: Amplicons from Zt_gen (shorter), 1A5.5 (longer, upper rows) and 1A5.6 (longer, lower rows). Isolate 1A5 as positive control and 3D7 as negative control. First part of isolate labels consist of location (E = Eschikon), treatment (e.g. A), and replicate (e.g. 1); second part contains measurement line (x1 for x_1); third, time point (T1 for t_1); fourth, leaf layer (L1 = Flag); and finally the isolate itself (e.g. 1A1: leaf 1, area A, isolate 1).

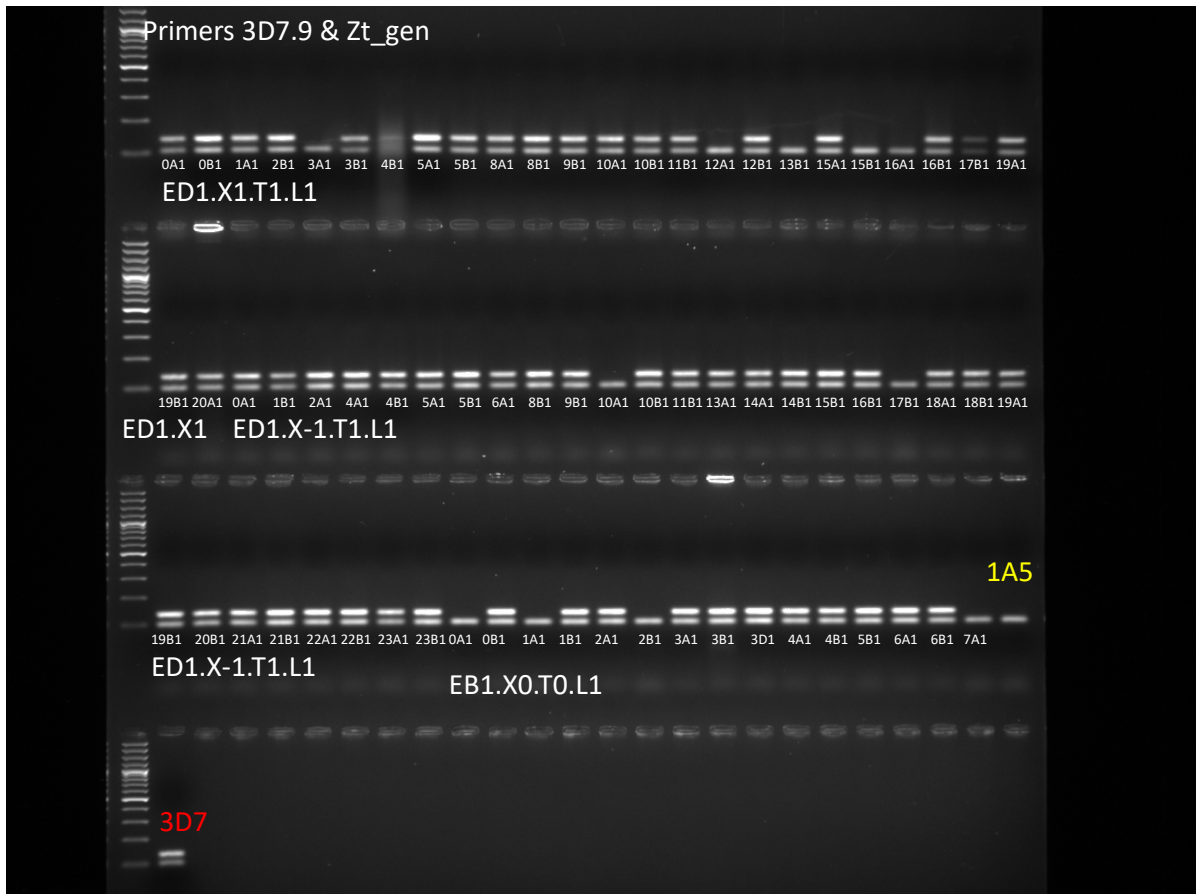


Figure C12: Amplicons from Zt_gen (shorter), 3D7.9 (longer). Isolate 3D7 as positive control and 1A5 as negative control. See Fig. C11 for label decoding.

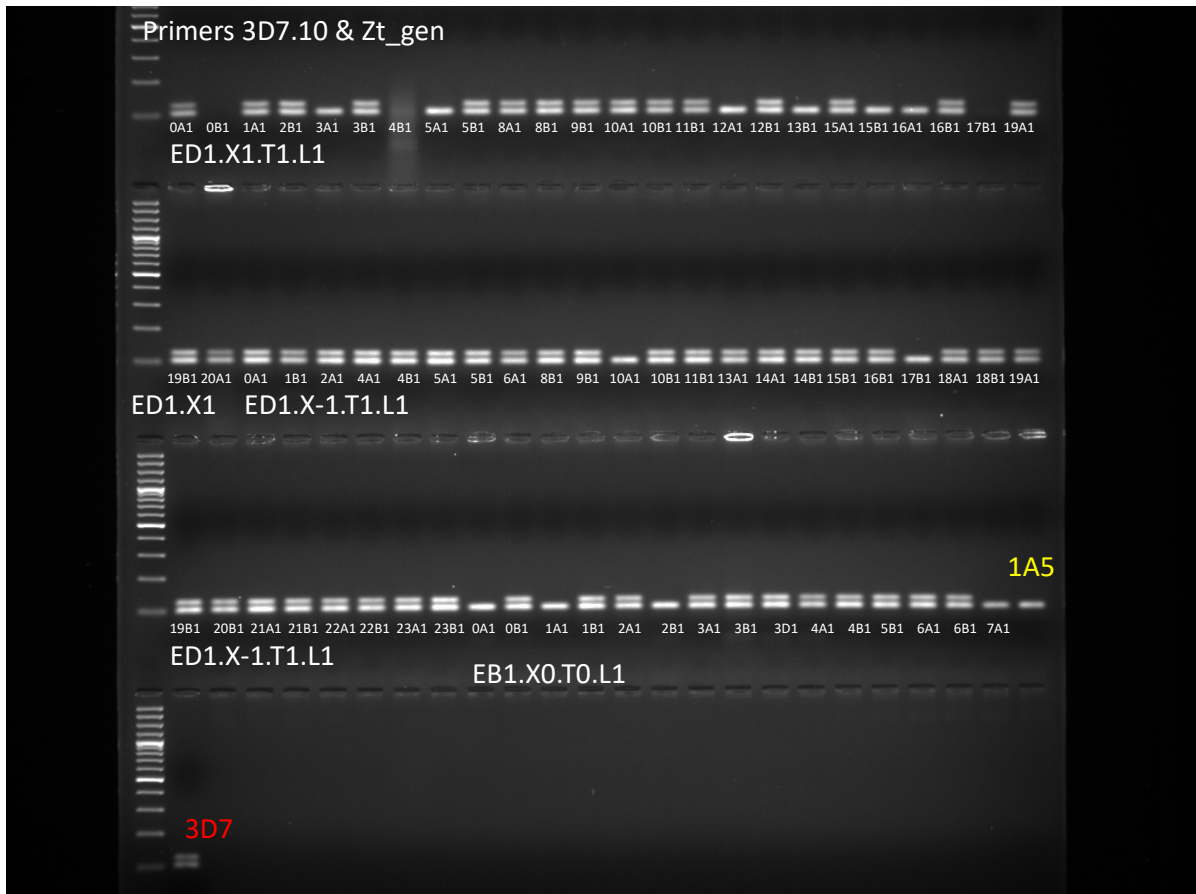


Figure C13: Amplicons from Zt_gen (shorter), 3D7.10 (longer). Isolate 3D7 as positive control and 1A5 as negative control. See Fig. C11 for label decoding.



Figure C14: Amplicons from Zt_gen (shorter), 1A5.5 (longer). Isolate 1A5 as positive control and 3D7 as negative control. See Fig. C11 for label decoding.



Figure C15: Amplicons from Zt_gen (shorter), 1A5.6 (longer). Isolate 1A5 as positive control and 3D7 as negative control. See Fig. C11 for label decoding.



Figure C16: Amplicons from Zt_gen (shorter), 3D7.9 (longer). Isolate 3D7 as positive control and 1A5 as negative control. See Fig. C11 for label decoding.

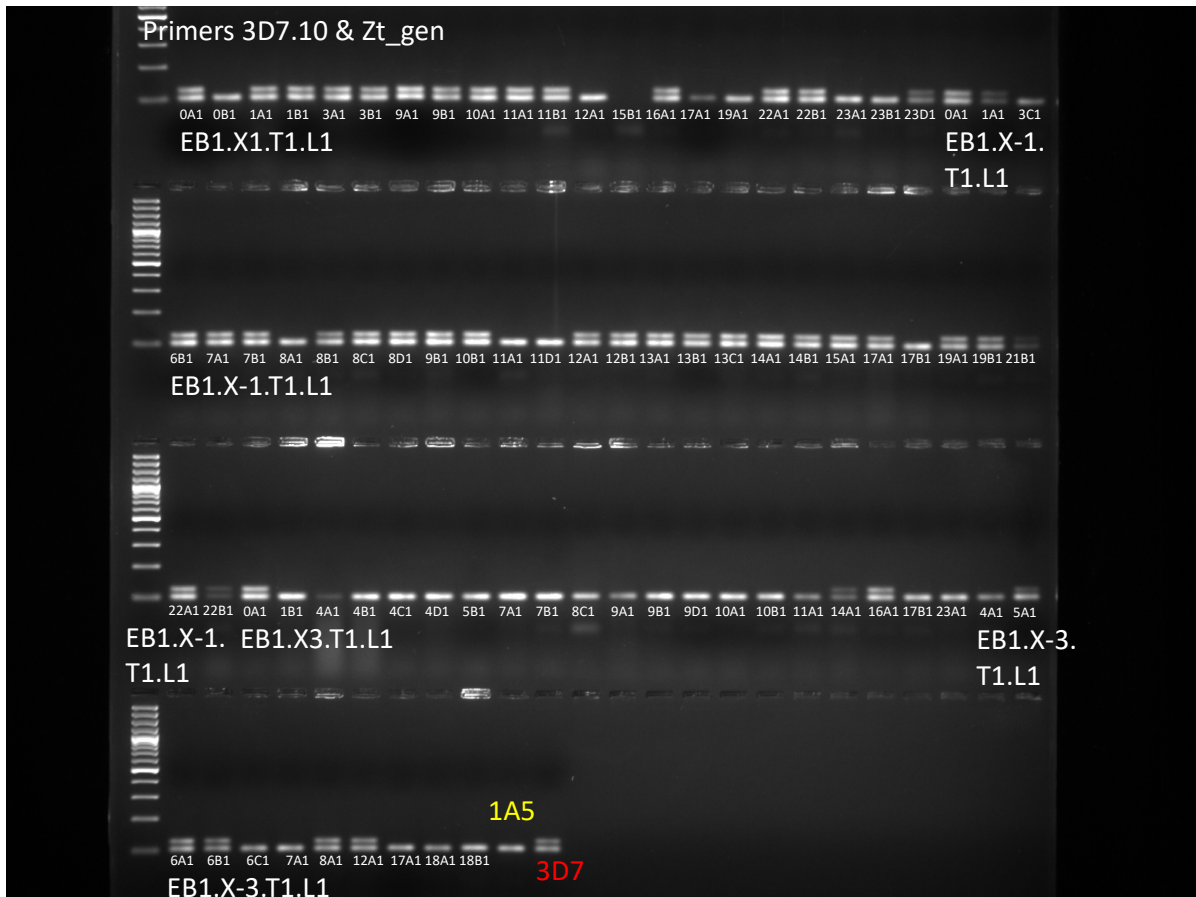


Figure C17: Amplicons from Zt_gen (shorter), 3D7.10 (longer). Isolate 3D7 as positive control and 1A5 as negative control. See Fig. C11 for label decoding.

818 Appendix D: Pictures of inoculation



Figure D1: P. Karisto setting up the inoculation tent on one plot.



Figure D3: A. Mikaberidze spraying the spore suspension inside the tent to inoculate the canopy of the source area.



820

Figure D2: Inoculation tent prepared.



822

Figure D4: A tent closed after inoculation to maintain high humidity.

Literature Cited

- 824 Akaike, H., 1973. Information theory and an extension of the maximum likelihood
principle. Pages 267–281 *in* B. Petrov and F. Csaki, editors. Proc. 2nd International
826 Symposium on Information Theory. Budapest.
- Bannon, F., and B. Cooke. 1998. Studies on dispersal of *Septoria tritici* pycnidiospores
828 in wheat–clover intercrops. *Plant Pathology* **47**:49–56.
- Brennan, R., B. D. Fitt, G. Taylor, and J. Colhoun. 1985. Dispersal of *Septoria nodorum*
830 pycnidiospores by simulated raindrops in still air. *Journal of Phytopathology* **112**:281–
290.
- 832 Brophy, L. S., and C. C. Mundt. 1991. Influence of plant spatial patterns on disease
dynamics, plant competition and grain yield in genetically diverse wheat populations.
834 *Agriculture, ecosystems & environment* **35**:1–12.
- Bullock, J. M., L. Mallada González, R. Tamme, L. Götzenberger, S. M. White, M. Pär-
836 tel, and D. A. Hooftman. 2017. A synthesis of empirical plant dispersal kernels.
Journal of Ecology **105**:6–19.
- 838 Bullock, J. M., K. Shea, and O. Skarpaas. 2006. Measuring plant dispersal: an intro-
duction to field methods and experimental design. *Plant Ecology* **186**:217–234.
- 840 Carrasco, L., T. Harwood, S. Toepfer, A. MacLeod, N. Levay, J. Kiss, R. Baker, J. Mum-
ford, and J. Knight. 2010. Dispersal kernels of the invasive alien western corn rootworm
842 and the effectiveness of buffer zones in eradication programmes in Europe. *Annals of*
Applied Biology **156**:63–77.
- 844 Clark, J. S., M. Silman, R. Kern, E. Macklin, and J. HilleRisLambers. 1999. Seed disper-
sal near and far: patterns across temperate and tropical forests. *Ecology* **80**:1475–1494.

- 846 Cousens, R., and A. Rawlinson. 2001. When will plant morphology affect the shape of
a seed dispersal "kernel"? *Journal of Theoretical Biology* **211**:229–238.
- 848 D'Aloia, C. C., S. M. Bogdanowicz, R. K. Francis, J. E. Majoris, R. G. Harrison, and
P. M. Buston. 2015. Patterns, causes, and consequences of marine larval dispersal.
850 *Proceedings of the National Academy of Sciences* **112**:13940–13945.
- Davison, A. C., and D. V. Hinkley. 1997. *Bootstrap methods and their application*.
852 Cambridge university press.
- Dean, R., J. A. van Kan, Z. A. Pretorius, K. E. Hammond-Kosack, A. Di Pietro, P. D.
854 Spanu, J. J. Rudd, M. Dickman, R. Kahmann, J. Ellis, and G. D. Foster. 2012. The
Top 10 fungal pathogens in molecular plant pathology. *Molecular plant pathology*
856 **13**:414–430.
- Djidjou-Demasse, R., B. Moury, and F. Fabre. 2017. Mosaics often outperform pyramids:
858 insights from a model comparing strategies for the deployment of plant resistance genes
against viruses in agricultural landscapes. *New Phytologist* **216**:239–253.
- 860 Duncan, K. E., and R. J. Howard. 2000. Cytological analysis of wheat infection by
the leaf blotch pathogen *Mycosphaerella graminicola*. *Mycological research* **104**:1074–
862 1082.
- Duvivier, M., G. Dedeurwaerder, M. De Proft, J.-M. Moreau, and A. Legrève. 2013.
864 Real-time PCR quantification and spatio-temporal distribution of airborne inoculum
of *Mycosphaerella graminicola* in Belgium. *European Journal of Plant Pathology*
866 **137**:325–341.
- Emsweller, L. N., D. L. Gorchov, Q. Zhang, A. G. Driscoll, and M. R. Hughes. 2018.
868 Seed Rain and Disturbance Impact Recruitment of Invasive Plants in Upland Forest.
Invasive Plant Science and Management **11**:69–81.

- 870 Ferrandino, F. 1996. Length scale of disease spread: fact or artifact of experimental
geometry. *Phytopathology* **86**:806–811.
- 872 Fitt, B. D., H. McCartney, and P. Walklate. 1989. The role of rain in dispersal of
pathogen inoculum. *Annual review of phytopathology* **27**:241–270.
- 874 Fitt, B. D. L., P. H. Gregory, A. D. Todd, H. A. McCartney, and O. C. Macdonald.
1987. Spore dispersal and plant disease gradients; a comparison between two empirical
876 models. *Journal of Phytopathology* **118**:227–242.
- Golan, J. J., and A. Pringle. 2017. Long-distance dispersal of fungi. *Microbiology*
878 *spectrum* **5**:FUNK–0047–2016.
- Goto, S., K. Shimatani, H. Yoshimaru, and Y. Takahashi. 2006. Fat-tailed gene flow
880 in the dioecious canopy tree species *Fraxinus mandshurica* var. *japonica* revealed by
microsatellites. *Molecular Ecology* **15**:2985–2996.
- 882 Greene, D. F., and C. Calogeropoulos, 2002. Measuring and modelling seed dispersal
of terrestrial plants. Pages 3–23 *in* *Dispersal ecology: the 42nd symposium of the*
884 *British Ecological Society*.
- Hartmann, F. E., and D. Croll. 2017. Distinct trajectories of massive recent gene gains
886 and losses in populations of a microbial eukaryotic pathogen. *Molecular biology and*
evolution **34**:2808–2822.
- 888 Heald, F. 1913. The Address of the President for 1912: The Dissemination of Fungi
Causing Disease. *Transactions of the American Microscopical Society* **32**:5–29.
- 890 Henze, M., M. Beyer, H. Klink, and J.-A. Verreet. 2007. Characterizing meteorological
scenarios favorable for *Septoria tritici* infections in wheat and estimation of latent
892 periods. *Plant Disease* **91**:1445–1449.

- Johansson, R., P. Strålfors, and G. Cedersund. 2014. Combining test statistics and
894 models in bootstrapped model rejection: it is a balancing act. *BMC systems biology*
8:46.
- 896 Jones, E., T. Oliphant, P. Peterson, et al., 2001–. SciPy: Open source scientific tools
for Python. URL <http://www.scipy.org/>.
- 898 Jørgensen, L. N., M. S. Hovmøller, J. G. Hansen, P. Lassen, B. Clark, R. Bayles,
B. Rodemann, K. Flath, M. Jahn, T. Goral, J. H. Czembor, P. Cheyron, C. Maumene,
900 C. de Pope, R. Ban, G. C. Nielsen, and G. Berg. 2014. IPM Strategies and Their
Dilemmas Including an Introduction to www.eurowheat.org. *Journal of Integrative*
902 *Agriculture* **13**:265–281.
- Karisto, P., S. Dora, and A. Mikaberidze. 2019. Measurement of infection efficiency
904 of a major wheat pathogen using time-resolved imaging of disease progress. *Plant*
Pathology **68**:163–172.
- 906 Karisto, P., A. Hund, K. Yu, J. Anderegg, A. Walter, F. Mascher, B. A. McDonald, and
A. Mikaberidze. 2018. Ranking Quantitative Resistance to *Septoria tritici* Blotch in
908 Elite Wheat Cultivars Using Automated Image Analysis. *Phytopathology* **108**:568–
581.
- 910 Kema, G. H., D. Yu, F. H. Rijkenberg, M. W. Shaw, and R. P. Baayen. 1996. Histology
of the pathogenesis of *Mycosphaerella graminicola* in wheat. *Phytopathology* **86**:777–
912 786.
- Kirchgessner, N., F. Liebisch, K. Yu, J. Pfeifer, M. Friedli, A. Hund, and A. Walter. 2017.
914 The ETH field phenotyping platform FIP: a cable-suspended multi-sensor system.
Functional Plant Biology **44**:154–168.

916 Klein, E. K., A. Bontemps, and S. Oddou-Muratorio. 2013. Seed dispersal kernels
estimated from genotypes of established seedlings: does density-dependent mortality
918 matter? *Methods in Ecology and Evolution* **4**:1059–1069.

Loebach, C. A., and R. C. Anderson. 2018. Measuring short distance dispersal of
920 *Alliaria petiolata* and determining potential long distance dispersal mechanisms. *PeerJ*
6:e4477.

922 Lovell, D., S. Parker, T. Hunter, D. Royle, and R. Coker. 1997. Influence of crop growth
and structure on the risk of epidemics by *Mycosphaerella graminicola* (*Septoria tritici*)
924 in winter wheat. *Plant pathology* **46**:126–138.

Lovell, D., S. Parker, T. Hunter, S. Welham, and A. Nichols. 2004. Position of inoculum
926 in the canopy affects the risk of septoria tritici blotch epidemics in winter wheat. *Plant*
Pathology **53**:11–21.

928 Madden, L. V., G. Hughes, and F. van den Bosch. 2007. The study of plant disease
epidemics. American Phytopathological Society (APS Press).

930 McCartney, H., B. D. Fitt, and J. S. West, 2006. Dispersal of foliar plant pathogens:
mechanisms, gradients and spatial patterns. Pages 159–192 *in* B. M. Cooke, D. G.
932 Jones, and B. Kaye, editors. *The epidemiology of plant diseases*. Springer.

Morais, D., I. Sache, F. Suffert, and V. Laval. 2016. Is the onset of septoria tritici blotch
934 epidemics related to the local pool of ascospores? *Plant Pathology* **65**:250–260.

Mundt, C., and J. Browning. 1985. Development of crown rust epidemics in genetically
936 diverse oat populations: effect of genotype unit area. *Phytopathology* **75**:607–610.

Nathan, R., E. Klein, J. J. Robledo-Arnuncio, and E. Revilla, 2012. Dispersal kernels:
938 review. Chapter 15, pages 187–210 *in* J. Clobert, M. Baguette, T. G. Benton, and J. M.
Bullock, editors. *Dispersal ecology and evolution*. Oxford University Press Oxford.

940 Nathan, R., U. N. Safriel, I. Noy-Meir, and G. Schiller. 2000. Spatiotemporal variation
in seed dispersal and recruitment near and far from *Pinus halepensis* trees. *Ecology*
942 **81**:2156–2169.

Newton, A., G. Begg, and J. Swanston. 2009. Deployment of diversity for enhanced
944 crop function. *Annals of Applied Biology* **154**:309–322.

Newton, A., and D. Guy. 2011. Scale and spatial structure effects on the outcome of
946 barley cultivar mixture trials for disease control. *Field Crops Research* **123**:74–79.

Newville, M., T. Stensitzki, D. B. Allen, and A. Ingargiola. 2014. LMFIT: Non-Linear
948 Least-Square Minimization and Curve-Fitting for Python. Zenodo .

Robert, C., G. Garin, M. Abichou, V. Houlès, C. Pradal, and C. Fournier. 2018. Plant
950 architecture and foliar senescence impact the race between wheat growth and *Zy-*
moseptoria tritici epidemics. *Annals of botany* **121**:975–989.

952 Saint-Jean, S., M. Chelle, and L. Huber. 2004. Modelling water transfer by rain-splash
in a 3D canopy using Monte Carlo integration. *Agricultural and Forest Meteorology*
954 **121**:183–196.

Sapoukhina, N., Y. Tyutyunov, I. Sache, and R. Arditi. 2010. Spatially mixed crops
956 to control the stratified dispersal of airborne fungal diseases. *Ecological Modelling*
221:2793–2800.

958 Shaw, M. 1987. Assessment of upward movement of rain splash using a fluorescent tracer
method and its application to the epidemiology of cereal pathogens. *Plant Pathology*
960 **36**:201–213.

Shaw, M. 1990. Effects of temperature, leaf wetness and cultivar on the latent period
962 of *Mycosphaerella graminicola* on winter wheat. *Plant Pathology* **39**:255–268.

- Shaw, M., and D. Royle. 1993. Factors determining the severity of epidemics of *My-*
964 *cosphaerella graminicola* (*Septoria tritici*) on winter wheat in the UK. *Plant Pathology*
42:882–899.
- 966 Skarpaas, O., and K. Shea. 2007. Dispersal patterns, dispersal mechanisms, and invasion
wave speeds for invasive thistles. *The American Naturalist* **170**:421–430.
- 968 Skarpaas, O., K. Shea, and J. M. Bullock. 2005. Optimizing dispersal study design by
Monte Carlo simulation. *Journal of Applied Ecology* **42**:731–739.
- 970 Solheim, H., and A. M. Hietala. 2017. Spread of ash dieback in Norway. *Baltic Forestry*
23:144–149.
- 972 Soubeyrand, S., J. Enjalbert, A. Sanchez, and I. Sache. 2007. Anisotropy, in density
and in distance, of the dispersal of yellow rust of wheat: experiments in large field
974 plots and estimation. *Phytopathology* **97**:1315–1324.
- Stewart, E. L., D. Croll, M. H. Lendenmann, A. Sanchez-Vallet, F. E. Hartmann,
976 J. Palma-Guerrero, X. Ma, and B. A. McDonald. 2018. Quantitative trait locus
mapping reveals complex genetic architecture of quantitative virulence in the wheat
978 pathogen *Zymoseptoria tritici*. *Molecular plant pathology* **19**:201–216.
- Terpilowski, M., 2018. Scikit-posthocs. URL
980 <https://scikit-posthocs.readthedocs.io>.
- Torriani, S. F., J. P. Melichar, C. Mills, N. Pain, H. Sierotzki, and M. Courbot. 2015.
982 *Zymoseptoria tritici*: a major threat to wheat production, integrated approaches to
control. *Fungal Genetics and Biology* **79**:8–12.
- 984 Van Houtan, K. S., S. L. Pimm, J. M. Halley, R. O. Bierregaard Jr, and T. E. Lovejoy.
2007. Dispersal of Amazonian birds in continuous and fragmented forest. *Ecology*
986 *letters* **10**:219–229.

- Vidal, T., C. Gigot, C. de Vallavieille-Pope, L. Huber, and S. Saint-Jean. 2018. Con-
988 trasting plant height can improve the control of rain-borne diseases in wheat cultivar
mixture: modelling splash dispersal in 3-D canopies. *Annals of botany* **121**:1299–1308.
- Vidal, T., P. Lusley, M. Leconte, C. De Vallavieille-Pope, L. Huber, and S. Saint-Jean.
990 2017. Cultivar architecture modulates spore dispersal by rain splash: A new perspec-
992 tive to reduce disease progression in cultivar mixtures. *PloS one* **12**:e0187788.
- Werth, S., H. H. Wagner, F. Gugerli, R. Holderegger, D. Csencsics, J. M. Kalwij, and
994 C. Scheidegger. 2006. Quantifying dispersal and establishment limitation in a popu-
lation of an epiphytic lichen. *Ecology* **87**:2037–2046.
- 996 Zadoks, J., and F. van den Bosch. 1994. On the spread of plant disease: a theory on
foci. *Annual review of phytopathology* **32**:503–521.
- 998 Zadoks, J. C., T. T. Chang, and C. F. Konzak. 1974. A decimal code for the growth
stages of cereals. *Weed research* **14**:415–421.
- 1000 Zadoks, J. C., and R. D. Schein. 1979. *Epidemiology and plant disease management*.
Oxford University Press Inc.
- 1002 Zhan, J., G. H. Kema, C. Waalwijk, and B. A. McDonald. 2002. Distribution of mating
type alleles in the wheat pathogen *Mycosphaerella graminicola* over spatial scales from
1004 lesions to continents. *Fungal Genetics and Biology* **36**:128–136.
- Zhan, J., C. Mundt, and B. McDonald. 1998. Measuring immigration and sexual repro-
1006 duction in field populations of *Mycosphaerella graminicola*. *Phytopathology* **88**:1330–
1337.
- 1008 Zhan, J., C. Mundt, and B. McDonald. 2000. Estimation of rates of recombination and
migration in populations of plant pathogens—a reply. *Phytopathology* **90**:324–326.